IEEE Access
Multidisciplinary ⋮ Rapid Review ⋮ Open Access Journal

Received 10 July 2024, accepted 29 July 2024, date of publication 2 August 2024, date of current version 28 August 2024.

Digital Object Identifier 10.1109/ACCESS.2024.3437780

RESEARCH ARTICLE

Intelligent Fault Detection, Compensation, and Power Management in Microgrids: A Synchrophasor-Enhanced Approach Using Fuzzy Logic Controllers and RTDS

M. DHINU LAL AND RAMESH VARADARAJAN, (Member, IEEE)
School of Electrical Engineering, Vellore Institute of Technology (VIT), Vellore 632014, India
Corresponding author: Ramesh Varadarajan (vramesh@vit.ac.in)

This work was supported by the Vellore Institute of Technology.

ABSTRACT Microgrids are a viable approach for improving energy resiliency and sustainability. Current microgrid systems frequently suffer from inadequate fault identification and compensation techniques, resulting in operational inefficiencies and grid instability. Conventional control strategies may not effectively manage changing environmental conditions and variations in load, requiring a more adaptable and intelligent approach. The paper presents a sophisticated method that combines Fuzzy Logic Controllers (FLCs) with Synchrophasor Technology (ST) to tackle these challenges. This work aims to develop and execute a thorough solution for microgrids' fault identification, compensation, and power management. The paper proposed a MATLAB/Simulink model that includes a Solar Photovoltaic (SPV) system with an FLC-based Maximum Power Point Tracking (MPPT), a Diesel Generator (DG), a Battery Energy Storage System (BESS) with an FLC-based Battery Management System (BMS), a Voltage Source Inverter (VSI), and a Unified Power Flow Controller (UPFC) with a FLC. Phasor Measurement Units (PMUs) equipped with ST are used to monitor and identify the anomalies in the system. The analysis of the simulation data provides evidence of the efficacy of the suggested approach. The SPV system demonstrates strong performance in producing voltage and current, successfully adjusting to different irradiance levels. The MPPT algorithm based on FLC guarantees the highest power efficiency. Additionally, the BESS and UPFC, controlled by FLCs, enhance grid stability and power quality. By integrating with synchrophasor-enabled PMUs, the microgrid may achieve accurate fault detection, and thus, the operator can take corrective actions to guarantee dependable operation even under challenging circumstances. Furthermore, the reliability and efficiency of the proposed system were confirmed using a Real-Time Digital Simulator (RTDS) using RSCAD with PMUs in real-world environments. By employing hardware-based PMUs, the system can accurately monitor grid interactions in real-time, enabling prompt detection of disruptions and proactive deployment of control measures. The RTDS results showcased the system's ability to maintain grid stability and efficiently manage faults, as evidenced by the precise current and voltage magnitudes measurements and their phase angles, frequency, and Rate of Change of Frequency (ROCOF) during fault scenarios.

INDEX TERMS Solar photovoltaic, synchrophasor technology, phasor measurement units, real-time digital simulator.

The associate editor coordinating the review of this manuscript and approving it for publication was Vitor Monteiro.

I. INTRODUCTION

In recent years, the power sector has undergone significant restructuring due to the advancement of Renewable Energy

Sources (RES), storage systems for energy, and enhanced control technology. The development of integrated power systems (PS) may be traced back to the increasing worldwide focus on sustainable energy solutions and the environmental impacts of traditional energy generation. Although Solar Photovoltaic (SPV) systems were imagined in the mid-20th century when scientists started thinking about converting sunlight to electricity, the engineering principles of refining renewable energy extraction and usage grew in the 1970s, involving the oil crisis and the attention to alternative sources [1]. Subsequently, the technology has undergone significant advancements in material and production efficiency, rendering it one of its most widely adopted applications of energy from renewable sources.

The incorporation of SPV systems into microgrids is emerging as a recent trend, influencing the viability of off-grid decentralization. In the last few years, apparent growth in microgrids- small-scale energy systems that act independently or are integrated into the primary grid can be observed [2]. Such growth is facilitated by the increase in distributed energy resources, such as SPV systems, driven by the need for a more robust and flexible power infrastructure. Integrating Maximum Power Point Tracking (MPPT) approaches is essential to achieve optimal SPV system power output. The aim of the proposed study in [3] is to perform a comprehensive examination of 40 historical and current MPPT methods for SPV systems. The approaches are structured and systematized, allowing the reader to select the type of action most suitable for solving a particular problem. The paper is designed to facilitate the classification of various MPPT methods, offering a comparative table that will allow researchers dealing with SPV systems to understand the assortment and select the method suitable for a specific task force. The rapid development of SPV technology, Battery Energy Storage Systems (BESS) and power electronics have contributed substantially to the overall development of integrated systems. Over the past few years, the research and development in the power industry has been focused on the integration of renewable energy sources, such as SPV systems, with BESS and advanced control systems to deal with the intermittent and variable nature of RE generation and improve the PS performance [4].

The study in [5] introduces a two-step SPV technology incorporating battery storage. The DC-DC boost converter connects the solar array to the main Voltage Source Converter's (VSCs) DC link. Conversely, the secondary Voltage Source Converter (VSC) is linked with a bidirectional converter incorporating BESS. The power from the SPV array is controlled using an MPPT method that employs a Perturb and Observe (P&O) approach. The IEEE-519 standards ensure that the load voltage's Total Harmonic Distortion (THD) remains within the specified limits. The system performed excellently in static and dynamic scenarios, including handling solar insolation and load imbalance, ensuring efficient supply and power management. Nevertheless, the study failed to assess the resilience of the power control mechanism under various operational circumstances and disruptions, including variations in solar radiation, imbalances in load distribution, and load disturbances.

The researchers in [6] developed a Fuzzy Logic Controller (FLC) MPPT technique that relies on SPV's I-V and P-V characteristics. A new integrated parameter called 'Ea' was established to improve the accuracy and performance of MPPT under various environmental and operating situations. This parameter is derived from the I-V characteristic. This system maintained maximum peak power during low environmental conditions, where traditional algorithms exhibit poor tracking performance. It can also track the operating point as the source current region quickly travels from fully activated to partially activated during high and low irradiance transients. Nevertheless, the FL-MPPT algorithm's effectiveness was not showcased when subjected to diverse environmental factors, including varying temperatures, irradiation levels, and shading effects. No comparisons were made with other MPPT algorithms to determine its superiority in tracking efficiency and robustness. Another work in [7] presents a new non-isolated high step-up multi-port converter design in a standalone SPV-BESS-enabled PS. This work justifies multiport converters over single-input converters, resulting in simplified circuits, better efficiency, and reduced cost. The suggested multi-port converter achieves higher voltage gain, which boosts the SPV panel voltage and improves energy storage and use. Furthermore, the proposed multi-port converter offers a significant increase in voltage and a minimal Normalised Peak Inverse Voltage (NPIV) among semiconductor devices. Ultimately, it enables the MPPT technique to be applied to each SPV input source. A laboratory prototype with a power output of 240 W has been developed to showcase the practicality of the suggested multi-port converter. However, this work does not address the suitable control scheme or the poor performance under varying operating conditions and different types of renewable source energy and BESS.

Battery Management Systems (BMS) are significant for optimising Smart Energy Storage Systems (SESS) for energy from renewable sources. SESS is also critical for integrating renewable energy sources and peak decrease. A review of the BMS Strategies in renewable energy systems critically discusses the core aspects of the planned application and the optimisation techniques used by [8]. The examination categorises optimisation methodologies based on three areas. The types include directed search-based techniques, probabilistic techniques, and rule-based strategies. The work notes that the directed search-based methods are appropriate for solving optimisations on the financial objective, while the control strategies are used to resolve technical objective optimisations. BMS acts include state-of-charge estimates, cell balancing, and thermal management. Precise simulation and modelling of BMS are significant for increasing performance and promoting battery longevity.

Hybrid methodologies across various optimisation strategies are expected to drive the future formulation of operation plans.

The researchers in [9] propose an approach for resolving the optimal distribution and functioning of electricity generation from RES and BESS utilising the FL interface. The algorithm under consideration prioritises the efficient distribution and control of energy resources, using hourly data for one year. The suggested model depends upon the calculations of steady-state power flow and is intended for utilisation during the design phase to implement various RES and BESSs. The system has been set up on a test distribution system consisting of 37 nodes, resulting in an observed reduction of annual energy loss by 80% compared to the baseline scenario where no renewable source-based power is present. The findings of the testing phase, which involve various load curves, demonstrate that the optimally calibrated FLC can effectively adapt and sustain its effectiveness regardless of how the input data deviate from those utilised during the optimisation stage. Additionally, the performance of the approach is evaluated using data that was not employed throughout the optimisation process to assess the generalizability as well as the robustness of the study. Nevertheless, the authors fail to address their method's computing demands or time complexity, a crucial aspect to consider when contemplating practical implementation.

A microgrid Diesel Generator (DG) system identified in [10] is preferred in terms of Wind Energy Conversion Systems (WECS) because weather conditions do not affect production reliability. A DG is added to the microgrid to increase system reliability, especially in regions with unreliable grid connections. The WECS requires only wind availability, which is unreliable for low and high wind conditions. The DGs are available on demand to provide electricity when needed. It operates effectively at different loading levels compared to WECS. When used with an SPV system and BESS, the DG is better in hybrid system reliability due to simple control [11]. DGs demonstrate more efficacy when employed with the Unified Power Flow Controller (UPFC) for power flow regulation and grid reliability enhancement, in contrast to the WECS, which necessitates supplementary control measures for UPFC integration [12].

Flexible AC Transmission Systems (FACTS) devices are energy-based devices used in electrical PS to improve the controllability and stability of the grid. Utilising FACTS devices in a microgrid offers several benefits, including better voltage regulation, reduced power quality, improved dependence on the grid, and more efficient use of Distributed Energy Resources (DERs) [13]. FACTS devices enable PS characteristics to be regulated efficiently and precisely, promoting the seamless integration of RES and, as a result, microgrid efficiency, which also influences the robustness and adaptability of microgrid operations under different operating scenarios. According to [14], an approach to assessing the impact of BESS and FACTS technologies in the microgrid voltage profile and its stability is proposed. In particular, the authors analyze the use of the BESS with the SPV generation system, considering the busbar, which has the minimum voltage value in the system arranged. The usage of FACTS technologies is investigated as well. The IEEE 37-bus distribution test feeder is modelled and modified for study purposes. The research findings emphasised the significance of strategically positioning the BESS and FACTS devices in the microgrid to maximise their positive influence on voltage stability. The work shows meticulous analysis and planning are essential for optimising microgrid performance. In short, the results indicate that incorporating sophisticated energy transmission and storage technology can significantly improve the durability and effectiveness of contemporary power networks, especially as dispersed generation and RES continue to grow. However, the findings may not be applicable in the realistic microgrid, as it is difficult to examine all the variables that affect the microgrid's performance. The analysis solely focuses on the impact of BESS, SPV production, and FACTS devices on voltage stability and profile. It does not delve into other potential effects on microgrid effectiveness, such as power quality and system reliability.

The authors of [15] developed a supervisory controller that uses Fuzzy Logic (FL) to control the power of an isolated AC microgrid comprising RES, BESS, and loads. The FLC regulates the AC-bus frequency below its rating to curtail the power generation of the SPV system or to match the power generation of the auxiliary unit. It ensures that the battery's power and energy stay within the defined limits, preserving the steady flow of power. The efficiency of the FLC is demonstrated through the presentation of simulations and experimental findings. The MATLAB simulation model showed that the FLC efficiently regulates power flow. It maximises PV power when the bus frequency is equal to or below the standard frequency. Additionally, it reduces power output when the frequency exceeds the standard value. The results also indicated that the proposed method reduces auxiliary unit operation time, lowering operational costs while meeting load and battery demands. The experimental validation confirmed the real-time simulation results that the FLC regulated frequency between 49.5Hz and 50.5Hz. This regulation was achieved by automatically adapting to the feedback received from the two FLC subsystems.

Nevertheless, the paper fails to thoroughly examine the FLC's performance under different operating conditions and disturbances in microgrid systems. Moreover, the work fails to report any possible challenges or limitations arising when using the proposed controller in an actual microgrid system, such as communication time delays, hardware restrictions, or limited models of renewable sources. The experimental findings presented in the research are constrained to a particular microgrid setup that may not accurately reflect the controller's performance in diverse scenarios or with varying forms of RES.

The suggestion in [16] addresses the amalgamation of RES in the power systems and the challenges power engineers face in mitigating power quality issues. This study majorly analyses the applicability of FACTS controllers within the transmission and distribution systems. FACTS devices are crucial in enhancing voltage quality regulation, power quality shaping, power factor enhancement, system stability, and active power achievement while working as filters that reduce harmonics. However, this work focuses more on the FACTS controllers in a microgrid and smart grid setup, neglecting other potential applications or research areas at length. The paper lacks a more detailed analysis of certain test case studies or real-life applications of FACTS controllers in microgrid and smart grid systems.

Research reported in [17] also discusses a distinct work regarding microgrids' modelling and load behaviour. The work articulates that having an induction motor load related to an air conditioning system may cause dynamic voltage instabilities in microgrid systems. This research examines the analysis of dynamic voltage stability of microgrid systems during functional isolation by contingencies and the improvement achieved using FACTS devices like Distribution Static Compensators (DSTATCOM) and Static Var Compensators (SVC). The findings indicate that DSTATCOM outperforms SVC in improving dynamic voltage stability, reducing the time it takes for voltage to recover after a defect, and ultimately enhancing the operational durability of microgrids. The study examined the dynamic voltage stability of microgrid systems when they are operationally isolated owing to contingencies, and the two microgrid test systems with distinct topological characteristics were also carried out to evaluate the suggested technique. However, it does not thoroughly research the impacts of the different load types on the designed dynamic voltage stability of the microgrid. The implementation of the developed approach is experimentally limited to only two microgrid evaluation systems with different topological properties. As a result, it may not reflect the global population of microgrid systems found under real-world conditions.

The study presented in [18] provides a comprehensive analysis of current optimisation methods for determining the optimal positioning of installing FACTS in PS networks. In review, analysis of the classification of optimisation approaches is reported in four prevalent categories: classical, metaheuristic, analytic, and mixed or hybrid approaches. For various optimisation problems, classical optimisation is used most frequently; however, metaheuristic methods have received considerable attention owing to their efficacy in solving nonconvex constraints. Analytic methods focus on approaches and gradients, among which sensitivity analysis and optimisation are most prevalent. Mixed approaches produce better solutions by combining a variety of optimisation methods. Furthermore, the review provides a comparative analysis of the chosen methods' performances; however, there is no thorough study of each optimisation technique technology's distinctive challenges and constraints in generating datasets for FACTS device placement. This literature does not consider how different uncertainties and changes in PS affect the efficiency of FACTS devices optimized.

TABLE 1. Comparison of UPFC, SVC, STATCOM and TCSC in grid-connected systems.

Aspect	UPFC [12], [21], [23]	SVC [21], [23]	STATCOM [16], [23]	TCSC [22], [23]
Power flow control	Real and reactive power flow can be controlled effectively	Mainly reactive power control	Mainly reactive power control	Real and reactive power flow can be controlled effectively
Voltage regulation	Provides voltage support	Provides voltage support	Provides voltage support	Voltage instability, if not managed
Dynamic response	Fast response time	Moderate response time	Fast response time	Moderate response time
Compensation type	Both series and shunt compensation	Shunt compensation	Shunt compensation	Series compensation
System stability enhancement	Enhances transient stability	Improves transient stability	Enhances transient stability	Enhances transient stability
Integration with renewable sources	Supports integration of renewables	Supports integration of renewables	Supports integration of renewables	Supports integration of renewables
Control flexibility	Offers control over multiple parameters	Limited control parameters	Offers control over multiple parameters	Offers control over multiple parameters
Installation and maintenance	Requires complex installation and maintenance	Simpler installation and maintenance	Requires moderate installation and maintenance	Requires complex installation and maintenance
Cost	Generally higher cost	Moderate cost	Generally higher cost	Generally higher cost

The proposed works mentioned in [19] and [20] introduce the utilisation of a UPFC in conjunction with an FLC. Both works seem to focus more on grid systems' stability and dependability. The primary challenges faced by PS are eradicating faults and maintaining power quality. Introducing a three-phase fault into the microgrid assists in driving a faster reaction of the PS system in the occurrence of unfavourable conditions. To alleviate power quality issues, a FLC-based UPFC is used as FACTS device, to illustrate how advanced control systems optimises interruption levels and ensures steady power provision. The literature presents Table 1, which jointly demonstrates the possible advantages of using UPFC as the FACTS device over other devices in the proposed work [12], [16], [21], [22], and [23].

Incorporating Synchrophasor Technology (ST) utilising Phasor Measurement Units (PMUs) into the PS signifies an innovative approach for monitoring and quantifying fluctuations in the grid. Synchrophasors offer

real-time data on electrical quantities, allowing for accurate management and optimisation of the power system, in contrast to the typical Supervisory Control and Data Acquisition System (SCADA) measuring approaches.

The work proposed in [24] highlights the benefits of SPV systems for grid-connected microgrids, including their effectiveness, cost-effectiveness, and system size advantages. The study examines the use of PMUs in distributed generating systems for real-time grid monitoring and control. The goal is to enhance operational precision in power systems with many SPV units connected to the grid. The study evaluates PMU implementation for monitoring grid current and voltage during faults, proving its suitability for RES and the efficiency of the proposed control mechanism. The article introduces a synchronised control technique for an SPV system evaluated at various solar irradiation levels. The investigation reveals that the system works well under fault conditions. The PMU at the PCC in the electrical grid accurately detected failures, including L-G faults, with 0.2 to 0.8 seconds precision. The PMU properly monitored and analysed the power output of the SPV system and BESS while linked to the grid, ensuring reliable performance and stability during faults. The PMU charts showed a reduction in grid voltage from 180 V to 125 V during faults. The grid current was also monitored to pinpoint faults and ensure system stability. The empirical results validated the model for renewable energy sources, showed the strength and dependability of the suggested control technique, and showed that PMUs ensure reliable microgrid monitoring and management. The study's conclusions are primarily based on MATLAB/Simulink simulations. This simulation may not fully capture the complexities and variability of real-world situations, and the findings may be limited in generalizability.

Table 2 [25], [26], [27] examine the possible benefits of PMU compared to SCADA. ST improves the ability to observe and understand the microgrid, which helps make informed decisions and manage the system effectively. Synchrophasors can deliver accurate and coordinated measurements of current and voltage phasors and the Rate of Change of Frequency (ROCOF) within the microgrid. This capability allows for the real-time monitoring and management of the system [25]. One significant use is for fault detection, wherein PMUs enable the swift identification of defects inside the microgrid through their high-speed and synchronised measurements, which allows prompt response techniques, such as migrating the microgrid or isolating defective components, to guarantee less interruption and enhanced system dependability [28]. Furthermore, using real-time time-stamped data from PMUs is crucial to make well-informed judgements and effectively dynamically modify control parameters. In addition, incorporating PMU data into a Real-Time Digital Simulation (RTDS) improves the precision of the microgrid model. It enables the simulation of realistic scenarios, which eventually facilitates the advancement and evaluation of control systems and guarantees their efficacy in practical scenarios. The integration of synchrophasor-enabled PMUs yields a sophisticated and flexible microgrid system that possesses the ability to effectively react to dynamic fluctuations and disruptions which is proposed in this work.

TABLE 2. Advantages of PMU over SCADA.

Aspect	PMU	SCADA
Precision in measurement	High precision in synchronized measurement	Low precision data
Response time	Provides real-time data with high-speed response	The time of response may be slower
Data synchronization	Ensures data synchronization across the network	May suffer from data synchronization challenges
Event detection	Rapid detection of faults and events	Delayed and less accurate fault and event detection
Dynamic monitoring	Allows continuous monitoring of dynamic changes	Less ability to capture rapid variations
Modelling and simulation	Enhances accuracy in modelling and simulation	Lower accuracy in modelling and simulation
Adaptive control techniques	Supports adaptive control with real-time data	Less adaptive control strategies

The comprehensive literature review reveals a lack of thorough examination and comparison of various methodologies for achieving optimal power management in microgrids across various operational circumstances, including fluctuating solar power insolation levels, load deficiencies, and environmental conditions. The literature frequently presents novel technologies and controllers without conducting comprehensive performance evaluations across various contexts. The utilisation of various traditional controllers in the microgrid, as stated in the literature, presents several drawbacks like suboptimal performance in managing the non-linear and dynamic characteristics of microgrid components, limited flexibility to fluctuating operating conditions, and increased complexity in tuning as well as coordinating different control strategies.

Furthermore, the review fails to comprehensively evaluate the PS in real-time or use RTDS to withstand and adapt to different operating conditions. One notable deficiency in the existing literature is the limited exploration of various applications and areas of inquiry on FACTS controllers inside microgrid and smart grid environments. The review could not detect any study of the potential impact of uncertainties and variations in PS characteristics on the effectiveness of the optimised FACTS devices, hence neglecting a crucial issue. The works based on ST in conjunction with PMUs for monitoring and measuring the PS grid are also limited and yet to be explored. These gaps in the

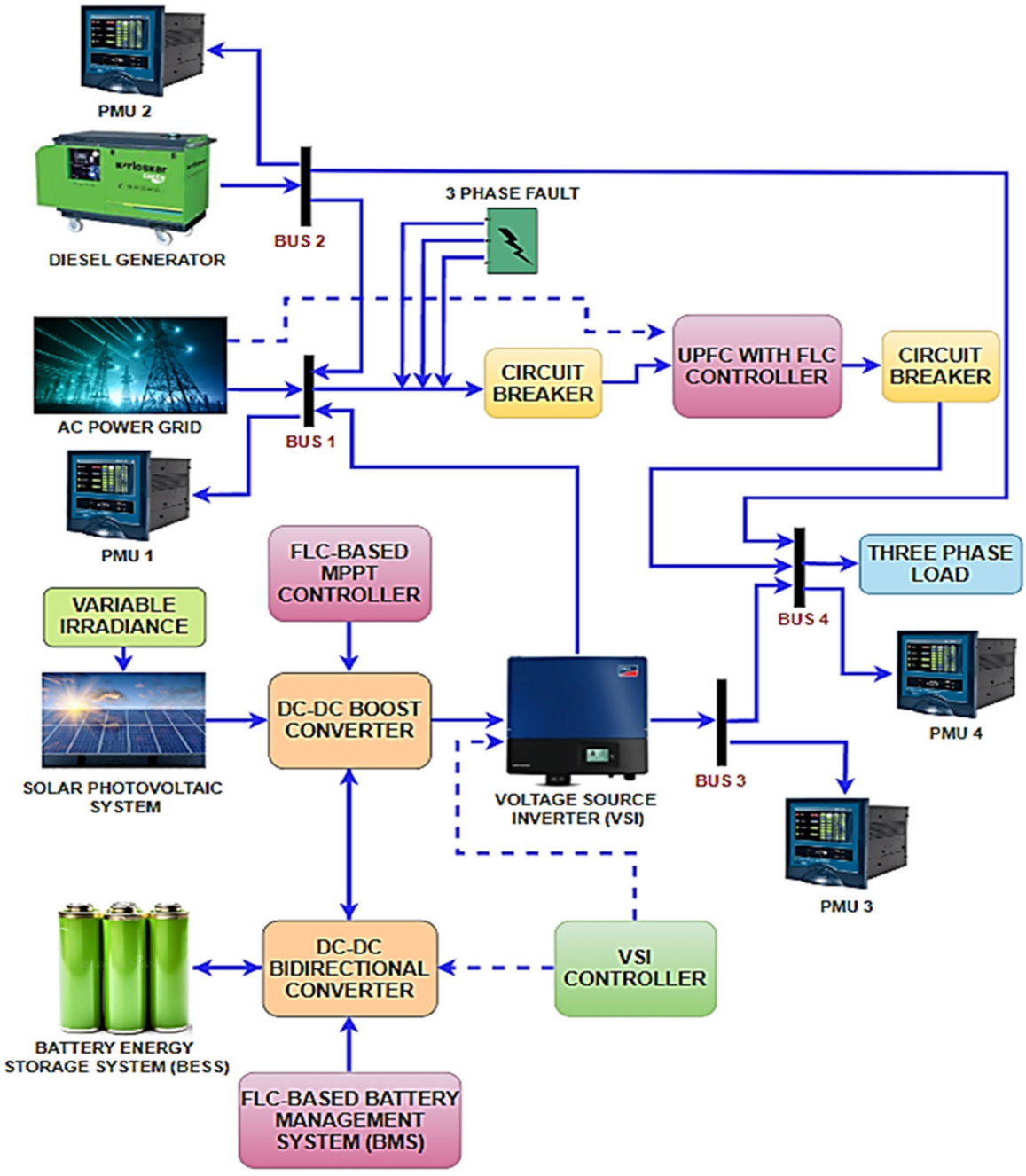

FIGURE 1. Functional block of proposed system.

existing body of literature underscore the necessity for conducting more extensive and varied studies to enhance the comprehension and use of intelligent power management in microgrids.

The primary approach of the proposed system is achieved by integrating an SPV system, an FLC-based MPPT system, the BMS with FLC, and a DG under consideration in the same microgrid in which PMUs are installed. Therefore, the proposed work offers an effective fault detection, compensation, and power management solution in modern PS. These RESs, innovative control systems, and power quality enhancement practices will make the entire power infrastructure more reliable, efficient, and sustainable. Moreover, this work intends to enhance the development and practical feasibility of integrating new systems by developing ST utilizing PMU in RTDS. Fig 1. shows the proposed system. The proposed work aims to achieve the following objectives.

- Design and develop a MATLAB/Simulink model that integrates a microgrid with an SPV system,

incorporating variable irradiance and employing an FLC-based MPPT approach.
- Design, model, and integrate a DG to ensure seamless integration and coordination with the grid and a BESS with FLC-controlled BMS to optimize the charging and discharging cycles.
- Design and implement a Voltage Source Inverter (VSI) and its controller, which can be utilized in microgrids for efficient power conversion.
- Design and implement a UPFC with FLC, enhancing the microgrid's power quality and grid stability.
- Analysis of internal fault detection, compensation, and power management in microgrids by installing synchrophasor-enabled PMUs from the performance plots obtained from MATLAB/Simulink.
- Validate and verify the performance by performing the synchrophasor-enabled PMUs in microgrids in RTDS using RSCAD and comparing the proposed method with existing literature.

The paper is organised as follows: Section II provides a detailed explanation of the methodology and modelling of the SPV system along with a boost converter, an MPPT controller that utilizes FLC, a BESS with DC-DC bidirectional converter, VSI as well as its controller, FLC-based BMS, DG, and AC power grid, UPFC with FLC controller, three-phase load and fault, PMUs, and their installation. In session III, the results obtained from the simulation in MATLAB/Simulink are analysed and examined. In Session IV, an analysis of simulation results is presented. In Session V, the validation process of the proposed system is done using the RTDS tool by applying RSCAD, and an analysis of the result is conducted. Session VI focuses on the work's novelty by comparing the results obtained from the proposed method with those of the existing literature. Session VII encompasses the discussion of the conclusion along with future work.

II. METHODOLOGY AND DESIGN

The design as well as modelling of the SPV system along with a boost converter, an MPPT controller that utilizes FLC, a BESS with DC-DC bidirectional converter, VSI as well as its controller, FLC-based BMS, DG, and AC power grid, UPFC with FLC controller, three-phase load with fault, and PMUs as well as their installation is conducted in this session from the functional block of the proposed system as depicted in Fig. 1.

A. MODELING OF SOLAR PHOTOVOLTAIC SYSTEM

The design and modelling of an SPV system reflect the overall approach of harvesting solar energy for electricity generation. The implementation of SPV in the system involves the application of SPV cells that assist in transforming solar radiation into electrical energy. A solar cell is the building block of an SPV system that converts sunlight into electrical energy through the photovoltaic process. Solar cells are often made of semiconductors, mainly silicon, which liberate electrons to move when exposed to sunlight. The PV activity begins with the interaction between solar radiation and the semiconductor material. The resultant effect of the interaction is the liberation of electrons from their atomic orbits [29]. Fig. 2 shows the circuit diagram of an SPV cell. The SPV cell operates by creating electricity from the liberated electrons' motion. The structure of the semiconductor material allows the creation of a voltage potential across the cell when an external circuit is connected. Electron movement is from the negative terminal to the positive terminal, where the current is generated by the electron movement that is DC in nature and usable as an output [30].

The Shockley equation, which denotes the diode behaviour, is expressed as follows:

$$I = I_{ph} - I_0 \left(e^{\frac{V+IR_S}{nV_t}} - 1 \right) \tag{1}$$

where I is the diode current, I_{ph} is the photo-generated current, I_0 is the diode reverse saturation current, V and R_S are the diode voltage and series resistance, n is the ideality factor, V_t is the thermal voltage and can be expressed as,

$$V_t = \frac{kT}{q} \tag{2}$$

where k is the Boltzmann constant, T and q are the temperature in Kelvin and electron charge, respectively.

The solar cell output power can be given by,

$$P_{out} = V * I \tag{3}$$

The SPV system efficiency becomes the ratio of the output power to the incident power and can expressed as,

$$\%\eta = \frac{P_{out}}{P_{incident}} * 100 \tag{4}$$

The incident power can be given as,

$$P_{incident} = G * A \tag{5}$$

where the variable G represents the amount of solar irradiation, while A denotes the cell area.

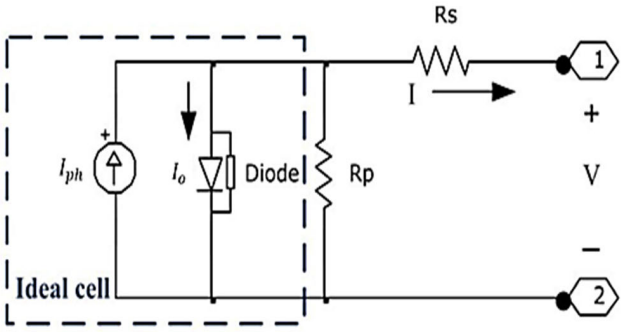

FIGURE 2. Circuit diagram of an SPV cell.

Because of First Solar FS-272's excellent performance, it is preferred in the proposed work. First Solar FS-272 incorporates state-of-the-art thin-film solar modules that exhibit outstanding performance when exposed to different environmental conditions. The thin film technology employed

TABLE 3. Design parameters of the SPV system.

Parameters	Values
Model	First Solar FS-272
Number of cells per module	116
Number of series-connected modules per string	2
Number of parallel strings	100
Voltage of the module at an open circuit	94.5738 V
Current of the module at a short circuit	1.18103 A
Voltage at maximum power	70.558 V
Current at maximum power	1.01088 A
Series resistance for one module	7.7692 Ω
Parallel resistance for one module	1044.9 Ω
Reverse saturation current	1.1116*e-68 A
Photo generated current	1.1898 A
Amplitude of irradiance	200, 500, 1000, 500, 200 kW/m2

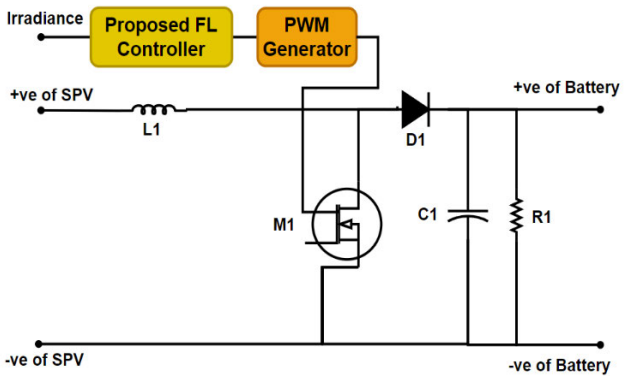

FIGURE 3. Circuit diagram of proposed DC-DC boost converter.

in these modules enhances energy generation, even under low light intensity, thus making the FS-272 a viable option where the weather is unpredictable, or sunshine is irradiant. The irradiance is set at various intensities for performance determination. A summary of the design specifications for the proposed First Solar FS-272 is given in Table 3.

B. MODELING OF DC-DC BOOST CONVERTER

The DC-DC boost converter is a power electronic block developed to raise the voltage of the DC power current from an SPV system. The device consists of an isolated switch MOSFET, diode, inductor, output capacitance, and resistance, as shown in Fig. 3. The boost converter functions by periodically establishing and severing the connection between the inductor and the input voltage, hence leading to an augmented output voltage [31].

A switch operation can be carried out in two primary modes: the on-state, characterised by a closed switch, and the off-state, characterised by an open switch [32]. When the switch M1 is in the On-state, it is closed, enabling the current flow via the inductor from the input voltage. During this period, the diode is in a state of reverse bias and does not exhibit conduction. Consequently, the energy is effectively stored within the inductor. During the off-state of switch M1, the switch is in a closed state, thereby severing the direct link between the input voltage and the inductor. Subsequently, the diode undergoes forward biassing, facilitating the passage of

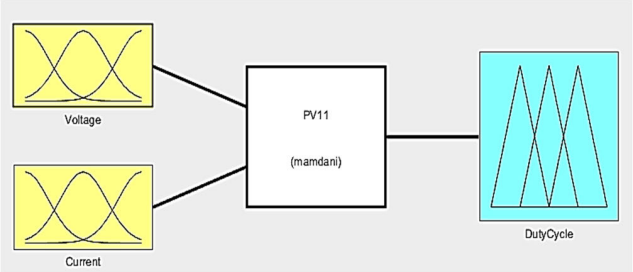

FIGURE 4. Proposed FLC designer for MPPT-based SPV.

inductor current through the diode and enabling the charging of the output capacitor.

Consequently, the resulting voltage will exceed the input voltage in this mode. The gate pulse supplied to the MOSFET switch is delivered via a Pulse Width Modulation (PWM) generator. The PWM generator is regulated by a controller based on FL, which will be elucidated in the upcoming session. The equations utilised explicitly for the design of a DC-DC boost converter are provided below.

The voltage across the inductor during on-state can be expressed as,

$$V_{Lon} = V_{in} - V_{out} \tag{6}$$

The voltage across the inductor during off-state is also given as,

$$V_{Loff} = -V_{out} \tag{7}$$

The duty cycle is the duration during which the switch is in the on-state. It is calculated by dividing the difference between the input and output voltages by the input voltage. The duty cycle is mathematically represented as:

$$D = \frac{V_{in} - V_{out}}{V_{in}} \tag{8}$$

C. MODELING OF MPPT CONTROLLER BASED ON FLC

Utilising MPPT to enhance the efficiency of SPV systems is a significant achievement. The present work proposed the employment of FLC, an intelligent control technique based on linguistic variables and human-centred logic, thus aiding in better decision-making [33]. The integration of MPPT tracking with FLC predominantly affects the performance of SPV systems. The MPPT algorithm changes the point of operation of the SPV panels level dynamically to optimize power generation, considering external variations such as temperature changes and shading impacts. FLC is designed to solve the same problem by using fuzzy rules to understand and respond to complex, non-linear relationships within the system, thereby improving its flexibility. FLC can deal with uncertainty and impreciseness associated with real-world situations and inaccurate data, making it suitable for practical applications. FLC also permits the ability to respond rapidly to solar irradiance and temperature changes. The FLC objective is to increase the power generation of an SPV system.

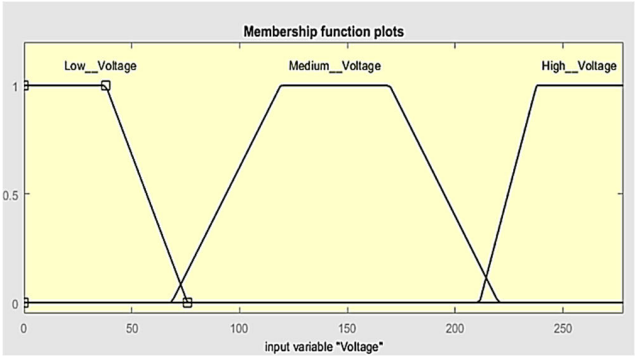

FIGURE 5. Membership function plot for input voltage.

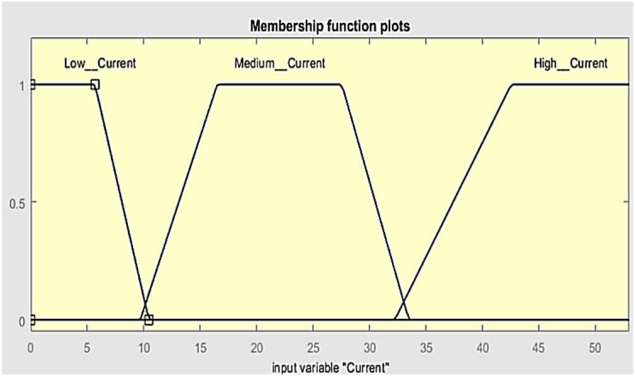

FIGURE 6. Membership function plot for input current.

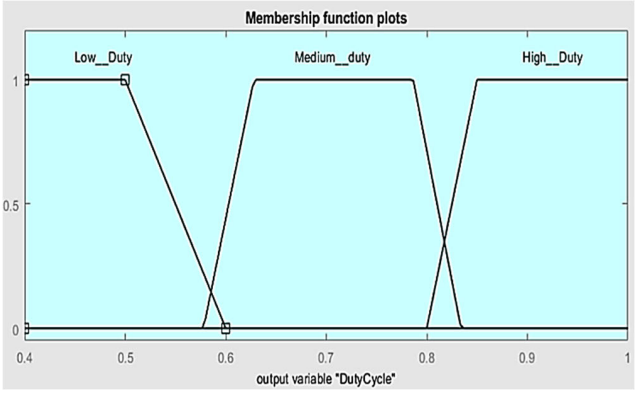

FIGURE 7. Membership function plot for output duty cycle.

It reaches this target by continuously adjusting the duty cycle of the boost converter. The FLC receives the current and voltage measurements from the SPV as inputs and generates the duty cycle as the output. The FLC algorithm applies the duty cycle to control the DC-DC boost converter since the duty cycle is utilized to control the converter [34].

The designed FL process is given in Fig. 4. A set of linguistic rules based on expert advice and experience is used to build the FLC. The following paths explain the relationship between the input variables, voltage and current, and the output variable, the duty cycle. The membership functions of the linguistic variables reveal essential properties

TABLE 4. Fuzzy rule table for proposed FLC-based MPPT for SPV systems.

Rule (If/And/Then)	Input Voltage	Input current	Output Duty Cycle
1	LV	LC	HD
2	LV	MC	MD
3	LV	HC	MD
4	MV	LC	HD
5	MV	MC	MD
6	MV	HC	MD
7	HV	LC	MD
8	HV	MC	LD
9	HV	HC	LD

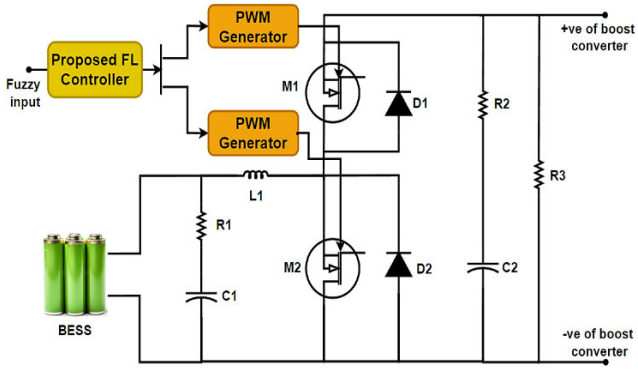

FIGURE 8. BESS circuit diagram featuring an FLC-based BMS and a bidirectional converter.

about the uncertainties and inaccuracies present in real-world situations. The PWM is used along with FLC to help the DC-DC converter accurately control the duty cycle of the MOSFET switches. The PWM is a technique extensively used in power electronics to stabilize the mean output voltage. The adjustment of the duty cycle is contingent upon the output of the FLC, which guarantees the efficient operation of the converter and its ability to follow the MPP of the SPV system accurately.

The case under consideration depicts the plot of the membership function for all three fuzzy sets of the input voltage, as shown in Fig. 5. The sets and their names in linguistic terms of input voltage as Low Voltage (LV), Medium Voltage (MV), as well as High Voltage (HV). Similarly, input current fuzzy sets are defined, as shown in Fig. 6, as Low Current (LC), Medium Current (MC), and High Current (HC). The fuzzy sets of the output variable duty cycle are defined as shown in Fig. 7 and are described in linguistic terms as Low Duty (LD), Medium Duty (MD), as well as High Duty (HD).

The fuzzy rule table in Table 4 represents the membership functions and rules within a Mamdani fuzzy system.

D. MODELING OF BATTERY ENERGY STORAGE SYSTEMS (BESS)

In the proposed study, integrating Lithium-Ion (Li-Ion) batteries with the BESS is critical to ensuring microgrid operations become more reliable and efficient. The BESS's primary energy storage element is the Li-Ion battery, which has high energy density per unit weight, extended cycle

life, and excellent charge/discharge characteristics. Integrating BESS to RES, especially in SPV systems, is crucial for offsetting due to their intermittent nature [35]. The DC-DC bidirectional converter is the system's component that allows the Li-ion battery to charge and discharge. The bidirectional converter facilitates battery charging during the high solar energy-producing periods, where the excess energy generated is stored for use during low-producing ones.

Additionally, during periods where the summed-up SPV system output and DG power are inadequate to fulfil the load demand, the BESS releases energy that was previously stored to fill the difference to enable the microgrid to provide an unabated and reliable power supply to the grid [36]. The operation of the BESS can be mathematically represented by the following equations, which dictate the system's battery charging and discharging processes. Fig. 8 shows the proposed BESS with a DC-DC bidirectional converter and FLC.

The battery voltage and current expression are given by,

$$V_{bat} = n_{cells} * V_{cell} \tag{9}$$

where, V_{bat} is the voltage of the battery, n_{cells} is the number of cells connected in series, and V_{cell} is the voltage of a single cell.

$$I_{bat} = \frac{V_{bat}}{R_{bat}} \tag{10}$$

where, I_{bat} is the current flowing through the battery and R_{bat} is the internal resistance of the battery.

The charge/discharge efficiency of the proposed BESS can be mathematically represented as,

$$\eta = \frac{Output\ Energy}{Input\ Energy} \tag{11}$$

The calculation of the State of Charge (SoC) for a Li-ion battery can be expressed as,

$$SoC\ (t) = SoC\ (t-1) + \frac{\Delta Q(t)}{Q_{max}} \tag{12}$$

Here $SoC\ (t)$ is the current state of charge at time t, $SoC\ (t-1)$ is the previous state of charge, $\Delta Q(t)$ is the change in charge at time t, and Q_{max} is the maximum capacity of the battery.

The energy stored in a battery is given as,

$$E_{Stored}\ (t) = \int_0^t P_{charging}\ (\tau)\, d\tau - \int_0^t P_{discharging}\ (\tau)\, d\tau \tag{13}$$

Here $E_{Stored}\ (t)$ is the amount of energy stored in the battery at time t, $P_{charging}\ (\tau)$ represents the power used for charging at time τ, and $P_{discharging}\ (\tau)$ is the power used for discharging at time τ.

The charging and discharging power equations are given by,

$$P_{charging}\ (t) = V_{dc}\ (t) * I_{charging}(t) \tag{14}$$

$$P_{discharging}\ (t) = V_{dc}\ (t) * I_{discharging}(t) \tag{15}$$

The variable $V_{dc}\ (t)$ represents the voltage that is applied across the DC bus (boosted solar PV) at a given time t. The variables $I_{charging}(t)$ and $I_{discharging}(t)$ denote the charging current and discharging current, respectively, at time t.

The selection of BESS design parameters is illustrated in Table 5.

TABLE 5. Design parameters of bess.

Parameters	Values
Type of battery	Lithium-Ion
Nominal voltage	400 V
Rated capacity	30 Ah
Initial SoC	100%
Maximum capacity	30 Ah
Fully charged voltage	512.1543 V
Nominal discharge current	13.0435 A
Capacity at nominal voltage	27.1304 Ah

E. MODELING OF DC-DC BIDIRECTIONAL CONVERTER FOR BESS

In microgrid systems incorporating RES, the DC-DC bidirectional converter facilitates batteries' charging and discharging processes [37]. Fig. 8 displays the bidirectional converter that has been suggested. The bidirectional converter transfers electrical power across the DC bus and the BESS, allowing for charging during periods of excess energy, such as peak solar generation, and discharging when the demand surpasses the generation capacity. An intelligent component is introduced into the system by incorporating an FLC into PWM control, enabling adaptive modifications in response to changing circumstances. The bidirectional converter functions in two primary modes: buck mode, which facilitates step-down conversion when charging, and boost mode, which enables step-up conversion during discharging. The bidirectional converter controls the voltage and current provided to the battery by the SPV and/or DG during the charging mode. The proposed FLC analyses input data, including battery SoC, grid voltage, and load demand, to dynamically modify the PWM signals, thereby optimising the charging process to enhance efficiency and battery health. The bidirectional converter facilitates the conversion of stored energy from the battery back into the DC bus during discharging. This conversion supports the microgrid, particularly during low renewable energy or high demand. The FLC is responsible for modifying the PWM signals following input parameters to achieve optimal power delivery while simultaneously upholding system reliability and stability [38]. In the design of a bidirectional converter, the expressions employed are as follows.

The voltage conversion ratio determines the relationship between the voltages at the input and output of the converter. It is provided by:

$$M = \frac{V_{out}}{V_{in}} \tag{16}$$

TABLE 6. Design parameters of DC-DC bidirectional converter.

Parameters	Values
Resistance of FETs	0.1 Ω
Snubber resistance of FETs	1*e5 Ω
Resistance of diodes	0.001 Ω
Forward voltage of diodes	0.8 V
Snubber resistance of diodes	500 Ω
Inductance	0.0001 H

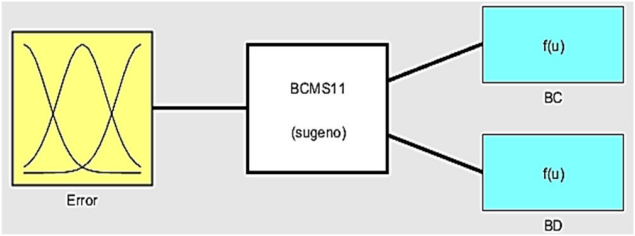

FIGURE 9. Proposed FLC designer for BMS.

The average output voltage of the converter can be determined by the duty cycle of the PWM signal and is given by,

$$D = \frac{T_{on}}{T_{total}} \tag{17}$$

Here T_{on} is the ON-time and T_{total} is the total switching period.

The inductor current ripple (ΔI_L) which is to consider for inductor sizing and converter efficiency and is given by,

$$\Delta I_L = \frac{V_{in}\,(1\text{-D})\,T_{sw}}{L} \tag{18}$$

Here T_{sw} is the switching period, and L is the inductance.

The output capacitor ripple current (ΔI_c) affects the output voltage ripple as well as the capacitor sizing and is expressed as,

$$\Delta I_c = \frac{V_{out}\,(1\text{-D})\,T_{sw}}{E * L} \tag{19}$$

Here, E represents the output capacitor's equivalent series resistance.

The average output voltage of a bidirectional converter can be calculated using,

$$V_{avg} = V_{in} * D \tag{20}$$

Table 6 presents the selected parameters for the design of the proposed bidirectional converter.

F. MODELING OF FLC-BASED BMS

The proposed study focuses on developing and implementing a BMS that incorporates an FLC within the context of a microgrid. The central component is an intelligent-based controller based on FL, created with the Sugeno block. The suitability of the Sugeno FLC for this particular application originates from its capacity to effectively manage non-linear systems and handle the inherent uncertainties present in microgrid scenarios [39]. Fig. 9 displays the FLC designer of the proposed BMS. The FLC receives inputs, applies FL rules to process them, and produces suitable outputs. In this scenario, the input to the FLC is the error signal obtained from the power output of the DC-DC boost converter that is part of an SPV system. Here, the error signal signifies departures from the intended power production, potentially arising from solar irradiance fluctuations or load variations. The FLC generates the control signals for battery charging and discharging operations. By examining the fault signal and using predetermined FL rules, the FLC can ascertain the suitable measures to uphold the ideal functioning of the battery. When the SPV system produces excess power, the FLC directs the BMS to retrieve the extra energy and store it in the battery for future use. On the other hand, in instances of increased demand or diminished solar power, the FLC instructs the BMS to release the battery, thereby supplying additional power to the microgrid [40].

The membership function plot, namely error, which is the input depicted in Fig. 10 of the proposed system, is classified

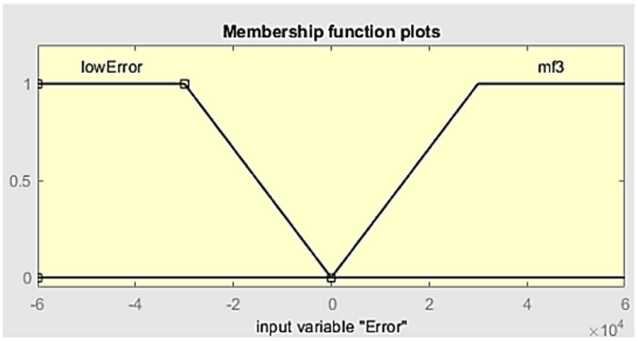

FIGURE 10. Membership function plot for input error.

TABLE 7. Fuzzy rule table for FLC-based BMS.

Rule (If/Then)	Error	Battery Charge (BC)	Battery Discharge (BD)
1	LE	mf1	mf3
2	HE	mf3	mf1

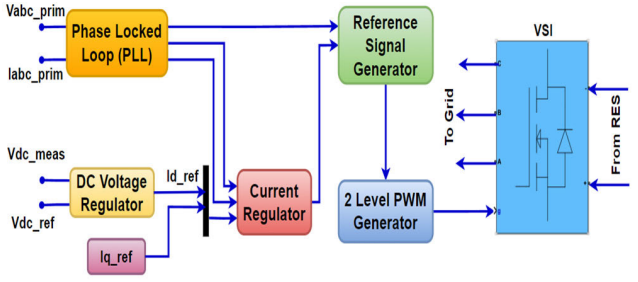

FIGURE 11. Block diagram of VSI and its controller.

TABLE 8. Design parameters for VSI.

Parameters	Values
Number of VSI bridge arms	3
Snubber resistance of VSI	1*e5 Ω
Resistance of VSI switch	0.001 Ω

into two distinct linguistic variables: Low Error (LE) and High Error (HE). The linguistic variables here indicate the extent of disparity between the intended and observed power outputs. The FLC's outputs are classified into two linguistic variables on battery operation: Battery Charging (BC) and Battery Discharging (BD). The linguistic variables utilised for charging and discharging are denoted as 'mf1' and 'mf3'. Table 7 displays a fuzzy rule table that demonstrates the decision-making process of the FLC, which shows a hierarchical arrangement wherein each row represents a distinct amalgamation of input linguistic variables (LE and HE), while each column represents a particular amalgamation of output linguistic variables (BC and BD).

G. MODELING OF VOLTAGE SOURCE INVERTER (VSI) AND ITS CONTROLLER

The VSI plays a crucial role in converting the DC power produced by the SPV and BESS into AC electricity for the grid-connected microgrid. The VSI converts the DC voltage obtained from these sources into a regulated AC voltage, guaranteeing that it is compatible with the microgrid's network. The proposed work utilises a VSI that employs power electronic switching MOSFET to provide an adjustable-frequency AC output from a constant DC input [41]. The conversion process is accomplished via a sequence of switching operations regulated by a PWM approach. Fig. 11 displays a VSI and its corresponding controller. The design parameters and the VSI specifications are provided in Table 8.

The VSI central controller gets multiple crucial inputs:

- The measured DC voltage V_{dc_meas} (440 V) across the VSI, ensuring consistent functioning within the specified voltage range.
- The grid current (I_{abc_prim}) and the grid voltage (V_{abc_prim}), which offers vital data regarding the current and voltage conditions of the grid and aids in the synchronisation of the grid and the injection of electricity.

To initiate the control process, the V_{abc_prim} and I_{abc_prim} undergo processing through a Phase-Locked Loop (PLL) to acquire $V_d V_{q\_prim}$ and $I_d I_{q\_prim}$. These signals correspond to the voltage and current components of the grid in a rotating reference frame synchronised with the grid's frequency along with its phase. Afterwards, the $V_d V_{q\_prim}$ and $I_d I_{q\_prim}$ that were obtained are inputted to a current regulator. The present regulator employs a PI controller with feedforward control to accurately control the current injected into the grid. In addition, a reference value named ($I_d I_{q\_ref}$) is given as input to the current regulator to control the desired current levels. The $I_d I_{q\_ref}$ is generated using a regulator. The regulator, which takes V_{dc} as its input, ensures that the DC link voltage remains at the appropriate level (440V) by employing a PI controller. The I_{d_ref}, which is the output of the regulator, is a component of the $I_d I_{q\_ref}$. The I_{d_ref} component is included in the $I_d I_{q\_ref}$ input as well. The current regulator effectively controls the active and reactive power flow by utilising the $I_d I_{q\_ref}$ as well as the measured current components.

A particular sign convention is utilised, wherein a positive current signifies power creation (inverter mode) or power absorption (inductive mode), accompanied by appropriate active (P) and reactive (Q) power values. The output of the current regulator is $V_d V_{q\_conv}$, representing the voltage components necessary to inject the intended current into the grid. After the PLL, the $V_d V_{q\_conv}$ signal and the angular frequency signal are then sent to a reference generator. This generator calculates the necessary voltage reference components to achieve the desired grid synchronisation and power injection. The reference voltage component signal is transmitted over a unit delay with a sampling interval of 5*e-5 seconds to attain accurate timing and synchronisation. Afterwards, the delayed signal is inputted into a PWM generator. The PWM generator utilises a 3-phase bridge with six pulses to produce the necessary gate pulses for controlling the switching of the VSI. The design characteristics and specifications of the VSI controller can be found in Table 9.

TABLE 9. Design parameters for VSI controller.

Parameters	Values
Nominal power of VSI controller	100*e3 VA
Nominal frequency of VSI controller	50 Hz
Nominal primary and secondary voltages of the controller	440 V
Nominal DC bus voltage	440 V
DC link voltage regulator gains (K_p, K_i)	7, 800
Current regulator gains (K_p, K_i)	0.3, 20

H. MODELING OF DIESEL GENERATOR

DG is an essential element of diverse power systems, offering dependable backup power during grid instability or serving as the main power supply in isolated regions. DG plays a pivotal function with several other sustainable energy sources and power management technologies [42]. The proposed DG system is powered by a 30 KVA, 3-phase synchronous generator. The diesel engine governor is responsible for managing the generator's rotational speed by controlling the diesel engine's speed. The governor consistently maintains a steady speed despite changes in load conditions, guaranteeing a stable output voltage and frequency. The speed control system has feedback systems to regulate fuel delivery in response to deviations from the desired speed setpoint.

Excitation control is a crucial element in the operation of synchronous generators. Excitation pertains to the level of magnetic field intensity in the rotor, which directly impacts the voltage produced by the generator. Within the framework of a DG system, the excitation system is responsible for guaranteeing that the generator generates the necessary voltage levels in various operational scenarios [43]. In this case, an automatic voltage regulator is used to modify the excitation current in response to variations in load and the system's needs. The equations employed for the design of a DG are as follows:

TABLE 10. Design parameters of a diesel generator.

Parameters	Values
3-phase synchronous generator	
Power	30 KVA
Line-to-line voltage (RMS)	350 V
Frequency	50 Hz
Stator resistance	0.0036 Ω
Inertia coefficient	1.07
Pole pairs	2
DG governor	
Regulator gain	40
Regulator time constants	0.01, 0.02, 0.2 Sec
Actuator time constants	0.25, 0.009, 0.0384 Sec
Engine time delay	0.024 Sec

The mathematical representation of the diesel engine governor is expressed as,

$$P_{ref} = P_{load} + P_{loss} \tag{21}$$

Here P_{ref} is the reference power, P_{load} is the actual output power and P_{loss} is the power loss, respectively.

The expression for excitation system is given by,

$$V_{ref} = K\left(V_{ref\ setpoint} - V_{terminal}\right) \tag{22}$$

Here, V_{ref} is the reference voltage for excitation, K is the excitation controller gain, $V_{ref\ setpoint}$ is the setpoint voltage, and $V_{terminal}$ is the terminal voltage, respectively.

The efficiency of a diesel generator is determined by,

$$\eta = \frac{Output\ power}{Input\ power} \tag{23}$$

The design parameters are shown in Table 10.

I. MODELING OF AC POWER GRID, THREE-PHASE LOAD AND FAULT

The proposed work aims to develop a thorough depiction of the AC power grid within the framework of a microgrid. This proposed methodology involves designing the power grid model, which includes many components such as a 3-phase source, transformers, and transmission lines. Moreover, it is essential to represent the three-phase load precisely, which is connected to the grid, to replicate its performance accurately under different operating situations. The model must include fault scenarios, such as short circuits and anomalies, to assess the system's performance in unfavourable conditions. This modelling stage establishes the basis for analysing the microgrid's fault identification, compensation, and power management strategies. The design parameters are presented in Table 11.

J. MODELING OF UPFC WITH FLC CONTROLLER

The UPFC is an integral component of the FACTS that performs a crucial role in enhancing the reliability and management of PS by effectively managing the flow of power, voltage, and impedance. The integration of two primary components, namely Converter 1 and Converter 2, is observed in this study. Converter 1 functions as a Static Synchronous

TABLE 11. Design parameters for a power grid, 3-phase load and fault.

Parameters	Values
3-phase AC source	
RMS values of line-to-neutral voltages	14434 V
Phase angles of line-to-neutral voltages	0, -120, +120 Deg.
Frequency	50 Hz
Internal source resistance	0.8929 Ω
Internal source inductance	0.01658 H
RMS value of internal base voltage (phase-to-phase)	63510.4 V
Transmission line parameters	
Number of phases	3
Line length	100 km
Frequency	50 Hz
Resistance per unit length	0.01273, 0.3864 Ω/Km
Inductance per unit length	0.0009337, 0.0041264 H/Km
Capacitance per unit length	1.274e-08, 7.751e-09 F/m
Three-phase Transformer (Inductance matrix type)	
Nominal power	100 kVA
Frequency	50 Hz
RMS values of line-to-line voltages	63510.4, 254.4 V
Winding resistances	0.01, 0.01 pu
No load losses (positive sequence)	1000 W
Short-circuit reactance (positive sequence)	0.06 pu
No load losses (Zero sequence) – Delta windings opened	1500 W
Short-circuit reactance (Zero sequence)	0.03 pu
3-phase load	
RMS value of nominal phase-to-phase voltage	440 V
Nominal frequency	50 Hz
Active power	300 kW
3-phase fault	
Switching time	0.1-0.3 Sec
Fault resistance	0.001 Ω
Ground resistance	0.01 Ω

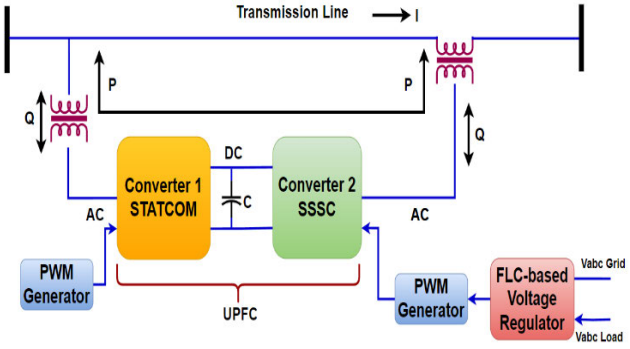

FIGURE 12. Circuit diagram of UPFC with FLC-based voltage regulator.

Compensator (STATCOM), while Converter 2 operates as a Static Synchronous Series Compensator (SSSC) [44]. These components are interconnected using a DC link capacitor. The suggested UPFC with an FLC-based voltage regulator is depicted in Fig. 12.

Converter 1, which functions as a STATCOM, utilises PWM techniques with the assistance of a PWM generator to regulate the injected reactive power within the system.

TABLE 12. Design parameters of UPFC.

Parameters	Values
Design of STATCOM	
Number of bridge arms	3
Power electronic device	Thyristor based
PWM generator type	3-phase bridge (6 pulse)
PWM generator frequency	1350 Hz
Initial phase of PWM	90 Deg
Modulation index of PWM	0.8
Design of SSSC	
Number of bridge arms	3
Power electronic device	Switching function-based VSC
PWM generator type	3-arm bridge (6 pulses)
Carrier frequency of PWM	2000 Hz
Voltage regulator proportional gain	0.6
Voltage regulator integral gain	4000
Three-phase Transformers – 2 Nos. (Inductance matrix type) for STATCOM and SSSC	
Nominal power	100 kVA
Frequency	50 Hz
RMS values of line-to-line voltages	254.03 V
Winding resistances	0.01, 0.01 pu
No load losses (positive sequence)	1000 W
Short circuit reactance (positive sequence)	0.06 pu
No load losses (zero sequence) – delta windings opened	1500 W
Short circuit reactance (zero sequence)	0.03 pu

This feature enables the flexible modification of voltage magnitude and the corresponding phase angle, effectively controlling the grid voltage while providing reactive power assistance as required. The gate pulses for Converter 1 are generated by the PWM generator, which guarantees precise control of the STATCOM's output voltage [45]. The STATCOM's output voltage is determined by,

$$V_{STATCOM} = V_{grid} + jX_{comp}I_{STATCOM} \tag{24}$$

Here, V_{grid} is the grid voltage, X_{comp} is the compensation reactance and $I_{STATCOM}$ is the current injected by the STATCOM.

Converter 2, operating as an SSSC, is employed to control the magnitude of the voltage at the load terminal and alleviate voltage fluctuations resulting from changes in the load and the grid. The gate pulses utilised in the SSSC switches are produced by an additional PWM generator that can be regulated by a voltage regulator based on an FLC. The regulator receives grid and load voltage as inputs and modifies the SSSC switching to uphold the appropriate voltage levels [45]. The formula for the output voltage of an SSSC is as follows:

$$V_{SSSC} = V_{load} + jX_{line}I_{SSSC} \tag{25}$$

Here, V_{load} is the load voltage, X_{line} is the line reactance and I_{SSSC} is the current injected by the SSSC.

In the UPFC system, the DC link capacitor functions as the energy storage component, guaranteeing seamless operation and supplying the required energy to the converters. To ensure the appropriate functioning of the converters, it is crucial to maintain the voltage within specific limitations. The manipulation of power flow between the converters allows voltage to be regulated across the DC link capacitor. This is accomplished by controlling the output voltages of the converters. The voltage across the DC link capacitor is given by,

$$V_{DC} = \frac{1}{C}\int (P_{STATCOM} - P_{SSSC})\,dt \tag{26}$$

Here C is the capacitance of the DC link capacitor, $P_{STATCOM}$ is the power flow through STATCOM and P_{SSSC} is the power flow through SSSC.

Table 12 provides the design parameters of UPFC.

The voltage regulation can be achieved by utilising an FLC employing the Mamdani block. Fig. 13 displays the system, which has been designed using the Mamdani model. In this configuration, the inputs consist of the grid voltage and the load voltage, while the output corresponds to the duty cycle of the UPFC. The objective of the FLC is to regulate the duty

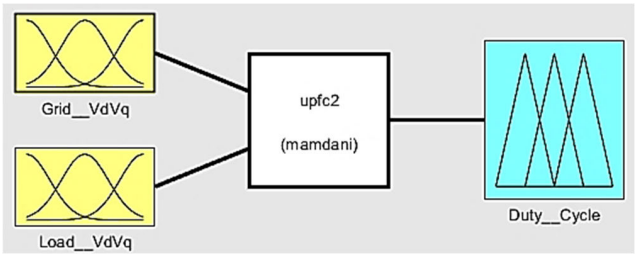

FIGURE 13. Proposed FLC designer for voltage regulator of UPFC.

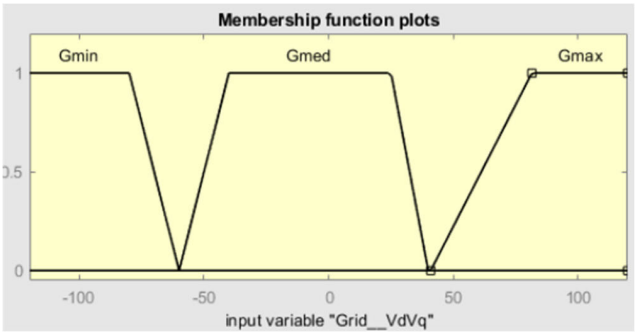

FIGURE 14. Membership function plot for input grid voltage.

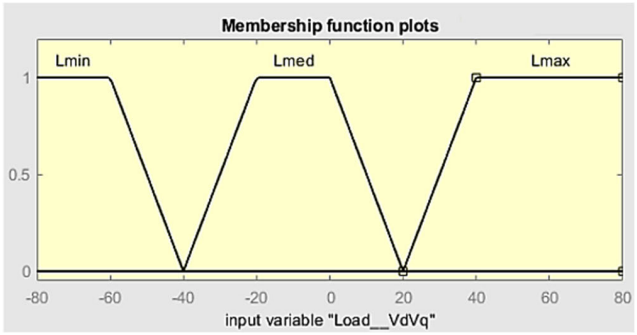

FIGURE 15. Membership function plot for input load voltage.

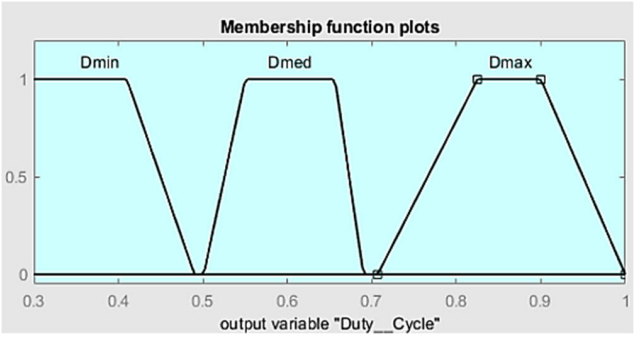

FIGURE 16. Membership function plot for output duty cycle.

TABLE 13. Fuzzy rule table for proposed FLC-based UPFC.

Rule (If/And/Then)	Input Grid Voltage	Input Load Voltage	Output Duty Cycle
1	Gmin	Lmin	Dmax
2	Gmin	Lmed	Dmax
3	Gmin	Lmax	Dmed
4	Gmed	Lmin	Dmax
5	Gmed	Lmed	Dmed
6	Gmed	Lmax	Dmin
7	Gmax	Lmin	Dmin
8	Gmax	Lmed	Dmed
9	Gmax	Lmax	Dmin

cycle dynamically by utilising the grid's measurements and load voltages to achieve optimal voltage control. The FLC is modelled by selecting parameters for both the input and output variables.

The factors responsible for determining the input grid voltage are the Grid Voltage Minimum (G_{min}), Grid Voltage Medium (G_{med}), and Grid Voltage Maximum (G_{max}). Fig. 14 displays a graph of the membership function for the input.

Fig. 15 displays the second membership function plot for the input load voltage, which encompasses parameters such as Load Voltage Minimum (L_{min}), Load Voltage Medium (L_{med}), and Load Voltage Maximum (L_{max}).

Fig. 16 displays the membership function visualisation of the output variable, duty cycle, which is defined by three parameters: Minimum Duty Cycle (D_{min}), Medium Duty Cycle (D_{med}), and Maximum Duty Cycle (D_{max}). The FLC functions by establishing a collection of fuzzy rules that dictate its decision-making procedure. Table 13 presents the fuzzy rule table.

K. MODELING OF SYNCHROPHASORS

ST's accuracy relies on using PMUs to precisely measure the magnitudes and phase angles of current, voltage, and the ROCOF at various locations within the electrical grid. The PMUs can sample data at high frequencies, generally reaching several kilohertz, allowing for the microgrid's real-time monitoring and management. GPS satellites are vital in PMU as they offer accurate timing data for synchronising measurements throughout the microgrid. The synchronisation of phasor measurements and anomaly detection is paramount [25].

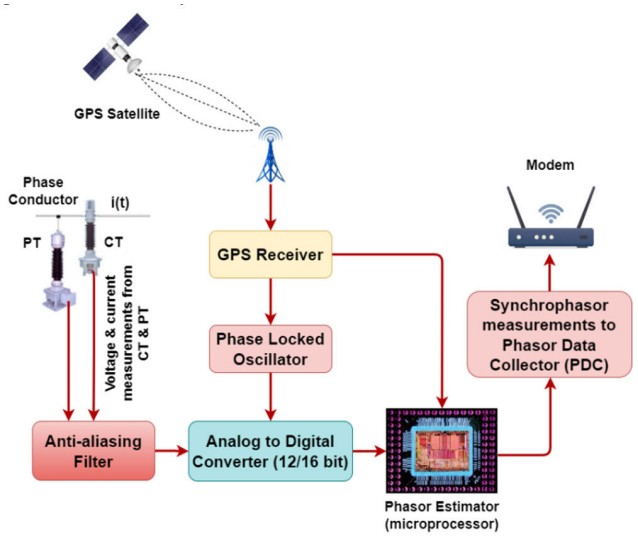

FIGURE 17. Standard block diagram of PMU.

TABLE 14. Design parameters of PMUs.

Parameters	Values
Type of PMUs used	PLL-based, positive sequence
IEEE standard	C37.118.1-2011
Nominal frequency	50 Hz
Sampling rate	64 point/cycle
Reporting rate factor	1

Fig. 17 depicts a standard block diagram of a PMU in a grid-connected system.

Potential Transformers (PTs) and Current Transformers (CTs) are utilised to acquire voltage and current data. These devices aim to reduce the elevated voltage and current levels within the microgrid to easily manageable levels for measuring purposes. The CTs and PTs measurements are subsequently inputted into an analog-to-digital converter that converts the signals into digital format for subsequent analysis. An anti-aliasing filter prevents aliasing and provides a precise digital representation of the analogue signals. This filter effectively eliminates high-frequency components that exceed the Nyquist frequency to mitigate distortions in digital signals. A phase-locked oscillator produces steady clock signals to achieve synchronisation and timing inside the system. It guarantees synchronisation across all components, preserving consistency in the measurements acquired from various places inside the microgrid. In the microgrid, the GPS receiver receives signals emitted by GPS satellites, enabling accurate measurement synchronisation. The synchronisation allows for precise estimation of the phasor and simplifies the process of monitoring and controlling the microgrid in real time. The phasor estimators are utilised to calculate phasor values by processing synchronised voltage and current measurements. Subsequently, the phasor readings are communicated to a Phasor Data Collector/Concentrator (PDC) to facilitate centralised processing and analysis. Ultimately, a modem enables the transmission of data and control orders

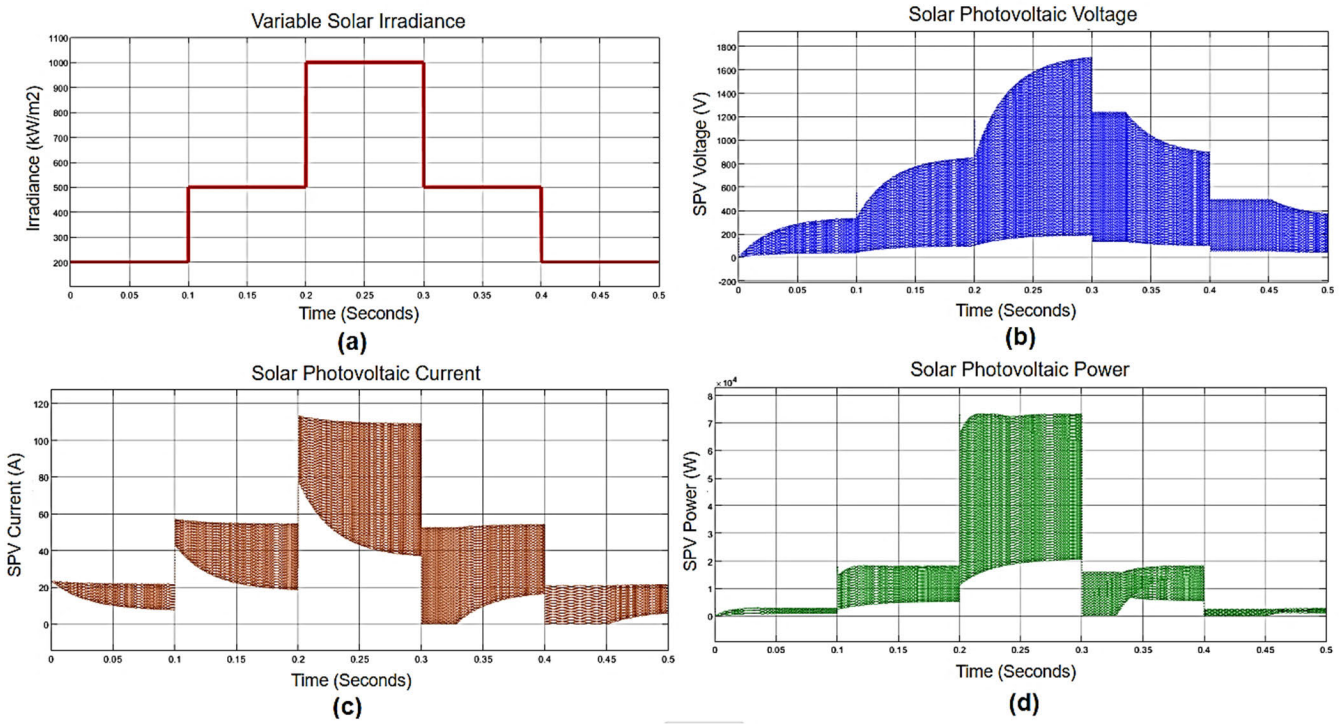

FIGURE 18. Performance analysis plot for SPV system. (a) Variable solar irradiance, (b) Solar PV voltage, (c) Solar PV current and (d) Solar PV Power.

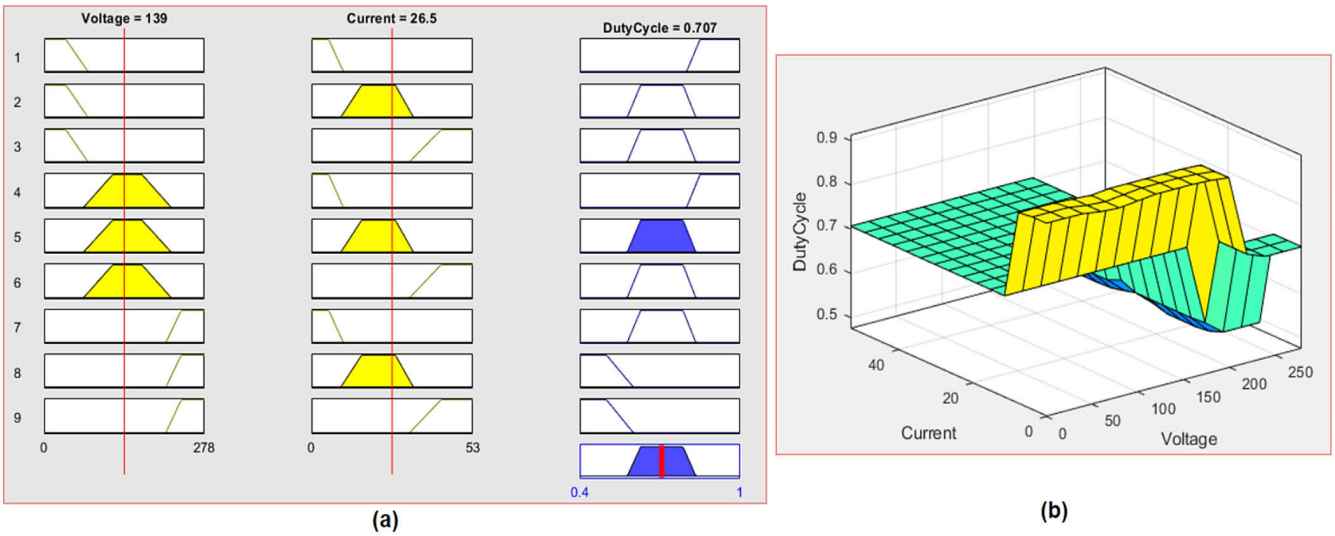

FIGURE 19. FLC-based MPPT design plots. (a) Fuzzy rule viewer, (b) Fuzzy surface viewer.

among the PDC and external systems [46]. Overall, using ST, the proposed system facilitates the incorporation of control algorithms, such as FLCs, to detect faults, provide compensation, and manage electricity inside the microgrid intelligently.

The proposed study employs four PMUs: the first PMU in the AC power grid bus, the second PMU in the DG bus, the third PMU in the SPV-BMS-inverter bus, and the fourth PMU in the load side bus. The PMUs are utilised to correctly monitor and measure voltages' magnitudes, currents, phase angles, and frequency. This enables the detection of abnormalities and faults at a more precise level, hence ensuring the system's stability. Table 14 displays the selected parameters for the design of PMUs.

III. SIMULATION RESULTS AND DISCUSSIONS

The primary objective of the proposed system is to enhance fault detection, compensation, and power management in microgrids using proposed FLCs and ST,

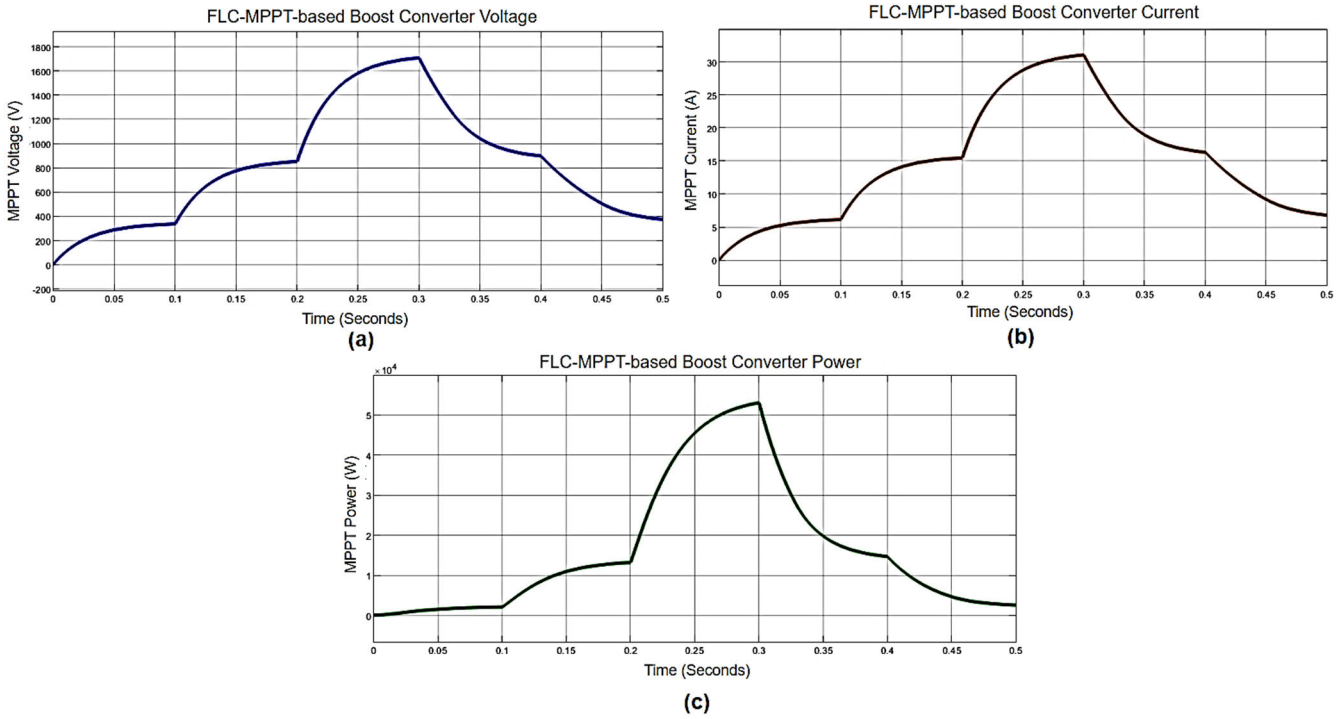

FIGURE 20. FLC-based MPPT output plots. (a) FLC-based MPPT DC-DC boost converter voltage, (b) FLC-based MPPT DC-DC boost converter current, (c) MPPT boost converter power using FLC.

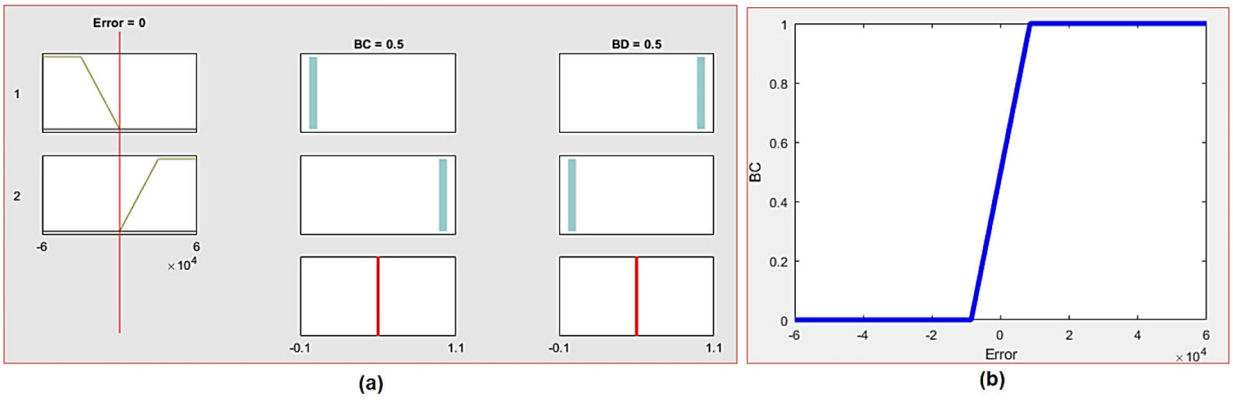

FIGURE 21. FLC-based BESS-BMS design plots. (a) Fuzzy rule viewer, (b) Surface viewer.

employing PMUs. The microgrid simulation is conducted using MATLAB/Simulink version R2023a, employing a halt time of 0.5 seconds. The system under consideration comprises an SPV system equipped with FLC-based MPPT. Furthermore, the system incorporates a BESS with a BMS managed by FLC to enhance its efficiency. In the event of grid instability, the system is equipped with a DG as a backup power source. Additionally, it can function as the primary source of electricity in remote areas, hence playing a crucial role in power management within the planned microgrid. An anomaly occurs during the time frame of 0.1 to 0.3 seconds, and its impact on the system is then examined. A UPFC is incorporated into the system to enhance the power quality of the grid, both during stable and defective conditions. Ultimately, the system's performance is monitored, and anomaly detections are seen through integrated PMUs inside the system. The subsequent sessions will delve into the examination of various plots acquired and their corresponding observations.

A. PERFORMANCE ANALYSIS OF THE SPV SYSTEM PLOTS

Fig. 18 (a) illustrates the design of the SPV system for a First Solar FS-272 model, incorporating variable irradiance levels of 200, 500, 1000, 500, and 200 kW/m2. The voltage plot, as depicted in Fig. 18 (b), is also acquired. The plot demonstrates that the proposed SPV model can create

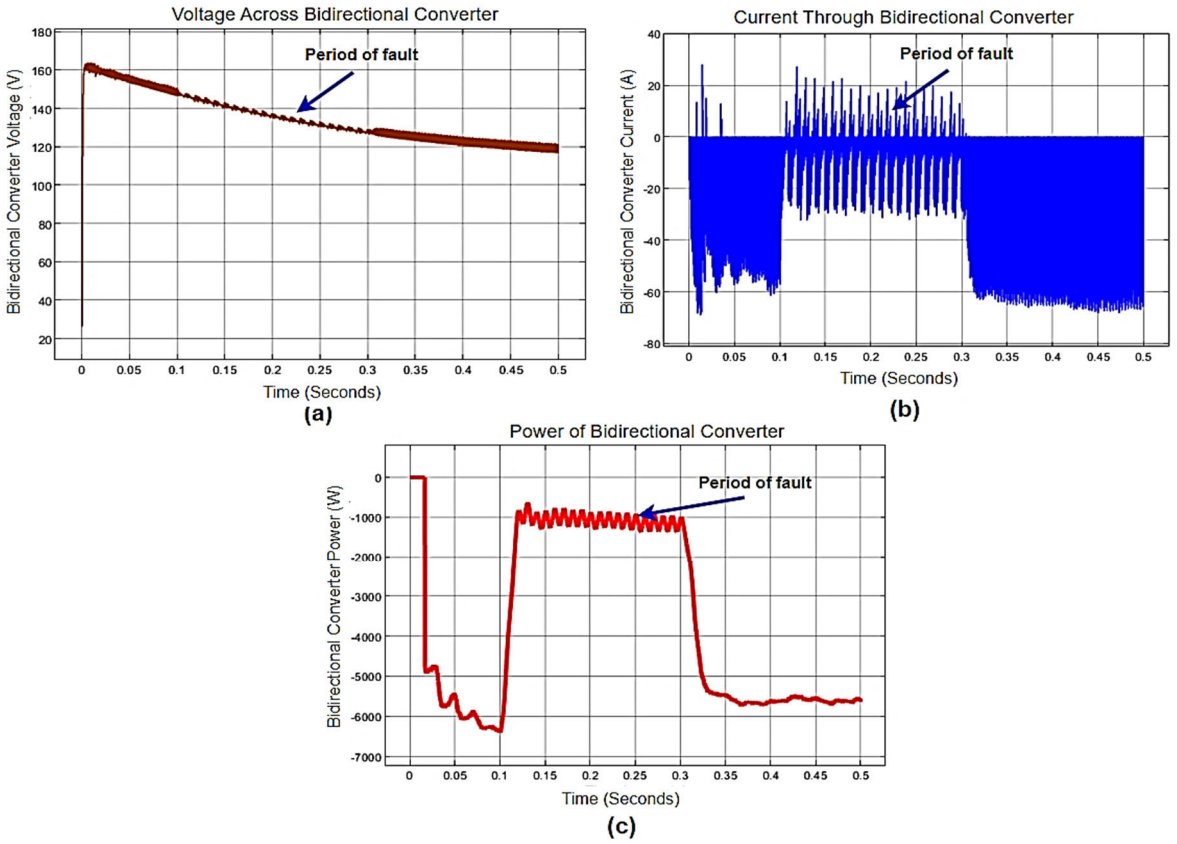

FIGURE 22. FLC-based DC-DC bidirectional output plots. (a) Voltage across bidirectional converter, (b) Current through bidirectional converter, (c) Power of bidirectional converter.

voltage by utilising changing irradiance, resulting in a peak voltage of 1700 V at a time interval of 0.3 seconds. The plot demonstrates the fluctuating voltage performance in response to different irradiation levels. The fluctuation of SPV current is depicted in Fig. 18 (c). It is evident from the image that the SPV also produces a fluctuating current in response to changes in irradiation. The proposed SPV system's power plot is computed and examined, revealing a peak power of 72 kW, as depicted in Fig. 18 (d). The power curve demonstrates that the proposed SPV can provide adequate power for a large microgrid system.

B. PERFORMANCE ANALYSIS OF FLC-BASED DC-DC BOOST CONVERTER PLOTS

The FLC plays a crucial role in the MPPT of the DC-DC boost converter-based SPV system. As an intelligent controller, the FLC efficiently regulates the power generated by the SPV system and utilises fuzzy rules to track the MPP accurately. Fig. 19 (a) displays the rule viewer of FLC-based MPPT. Fig. 19 (b) also presents a corresponding surface view plot.

The boost converter is incorporated into the system to increase the SPV system's voltage, even under fluctuating irradiance. The FLC-based MPPT plots are depicted in Fig. 20. The MPPT voltage is shown in Fig. 20 (a), illustrating the role of the FLC in regulating the duty cycle of the proposed boost converter. This adjustment ensures the output voltage remains ideal, facilitating maximum power transfer. Consequently, the voltage output demonstrates variations within a specific range, effectively monitoring the MPP of the proposed SPV array.

The output current of the boost converter is indicative of the MPPT operation in response to different environmental and load situations, as depicted in Fig. 20 (b). The input from SPV, such as temperature and irradiance, is continuously monitored by the FLC. Subsequently, the controller modifies the operational settings of the converter to enhance the ability to collect electric power from the solar panels. Considering variations in solar irradiance, load demand, and converter efficiency, the output current exhibits fluctuations, ensuring the maintenance of an ideal operating point for power generation.

Fig. 20 (c) illustrates the significant impact of the power output of the boost converter in the grid-connected SPV system on the overall performance of the MPPT control method. The FLC optimises power conversion efficiency by dynamically altering the operating point of the converter, hence maximising the power generated from the solar panels. The power output displays minor fluctuations in response to variations in irradiance levels, load demand, and

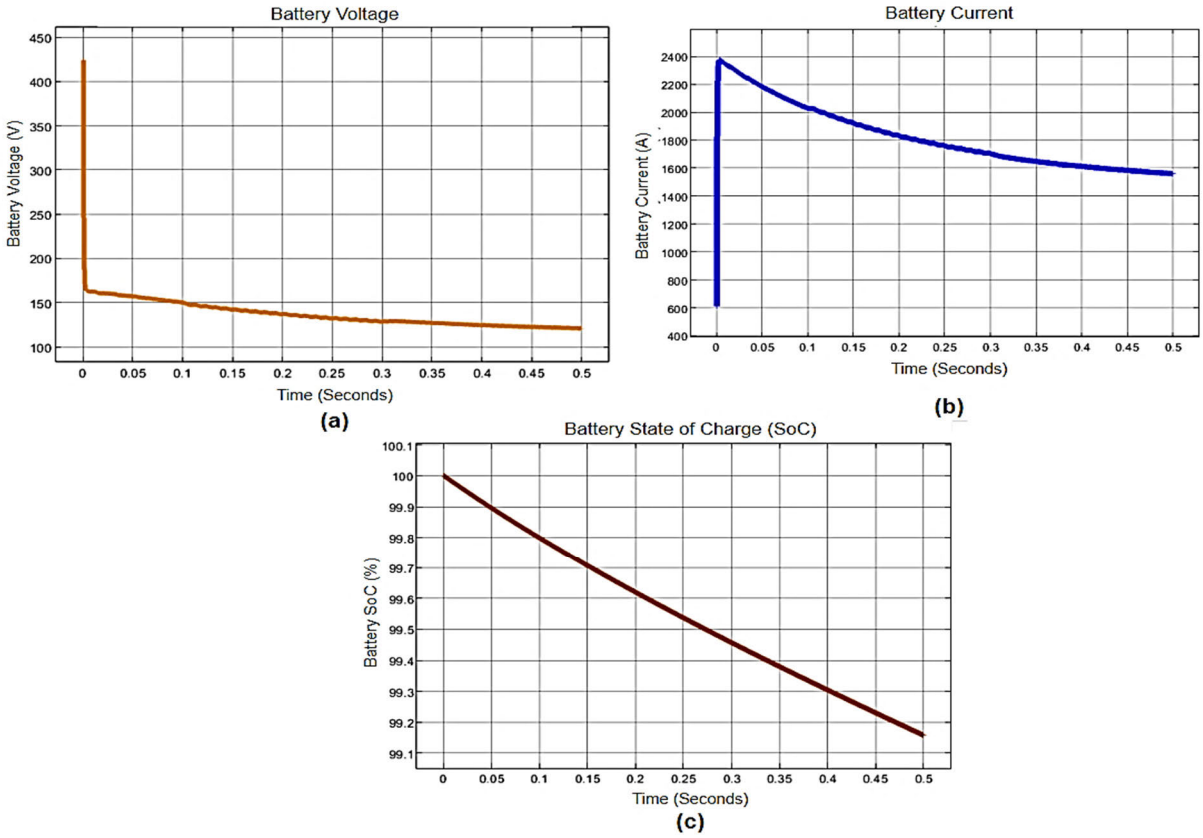

FIGURE 23. Battery performance plots. (a) Battery voltage plot, (b) Battery current plot and (c) Battery % SoC plot.

converter efficiency. However, it consistently maintains close to the MPP under most operating settings. Implementing this dynamic power output management mechanism guarantees optimal solar energy utilisation while preserving stability within the grid-connected system.

C. PERFORMANCE ANALYSIS OF BESS AND FLC-BASED BMS PLOTS

The MATLAB/Simulink results for a DC-DC bidirectional converter and BESS based on the FLC offer significant insights into their performance when subjected to fault scenarios. Fig. 21 displays the output of the FLC rule viewer and surface viewer. Fig. 22 illustrates the performance of the DC-DC bidirectional converter based on FLC. Under normal conditions, the FLC efficiently controls the voltage across the bidirectional converter, sustains the intended current through it, and regulates the power charging or discharging of the BESS. Nevertheless, the overall performance could be impacted if a fault occurs within the designated timeframe of 0.1 to 0.3 seconds. Fig. 22 (a) and (b) depict the voltage and current in the bidirectional converter, respectively. The analysis of the plots reveals that the occurrence of faults within this specific interval has the potential to cause disruptions in the system, showing abrupt variations in voltage and current. However, the FLC promptly addresses these disruptions and guarantees stability. The FLC can manage the system even when there is a defect and effectively preserve stability. The proposed FLC system's stability and efficacy are ensured by the power curve of the bidirectional converter depicted in Fig. 22 (c). During the fault phase, it is evident that the voltage across the converter undergoes transient spikes or falls, the current passing through it may display abrupt fluctuations, and the power entering or exiting the battery may depart from the intended setpoint.

It is observed from the plots that under typical circumstances, the BESS efficiently stores and releases energy under the specific demands of the system, so ensuring that its SoC remains within the desired thresholds. Nevertheless, if a malfunction arises during the designated timeframe, the efficiency of the BESS will be compromised.

Fig. 23 displays the performance curve of the FLC-based BMS. Failure can have several effects on the BESS, such as abrupt variations in voltage or excessive current, which might strain the battery cells, thereby impacting their durability and operational efficiency. Additionally, the problem can potentially interfere with the charging and discharging procedure, resulting in deviations in the SoC from the intended level. The FLC plays a crucial function in regulating the BESS during fault circumstances. Based on the analysis of the

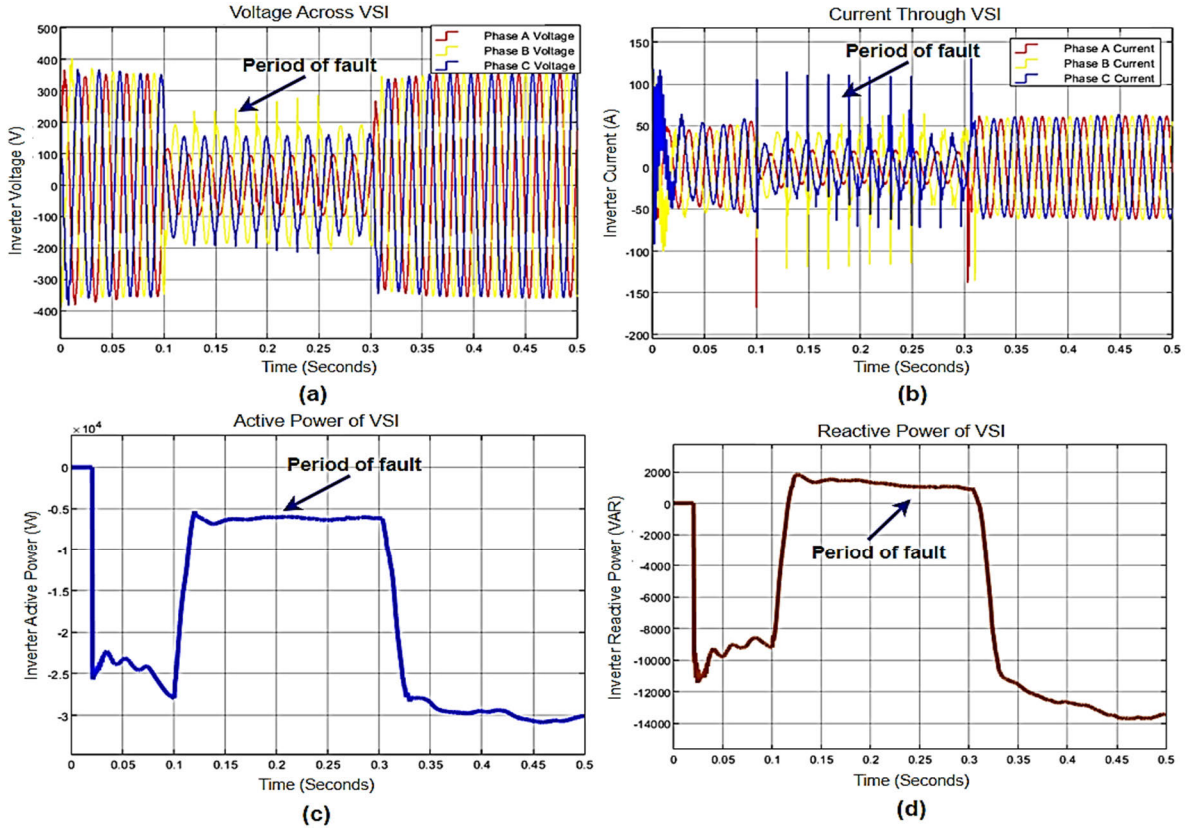

FIGURE 24. Performance analysis plots of VSI. (a) Voltage across VSI, (b) Current through VSI, (c) Active power of VSI, (d) Reactive power of VSI.

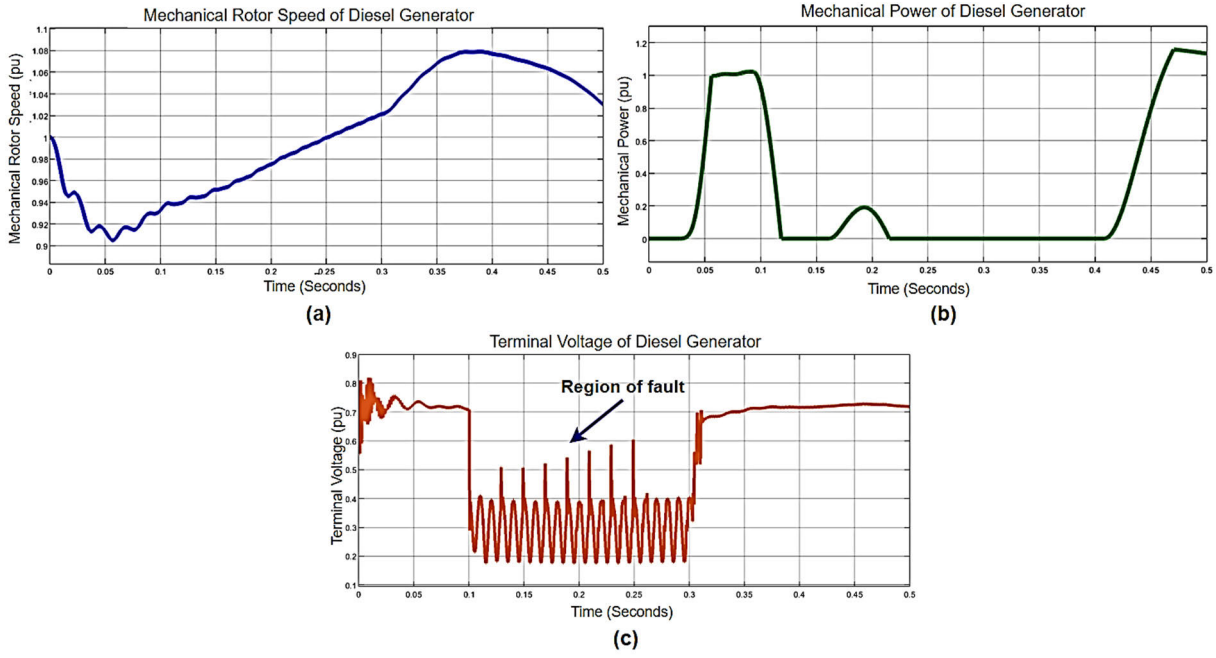

FIGURE 25. Diesel generator plots. (a) Mechanical rotor speed of diesel generator, (b) Mechanical power of diesel generator, (c) Terminal voltage of diesel generator.

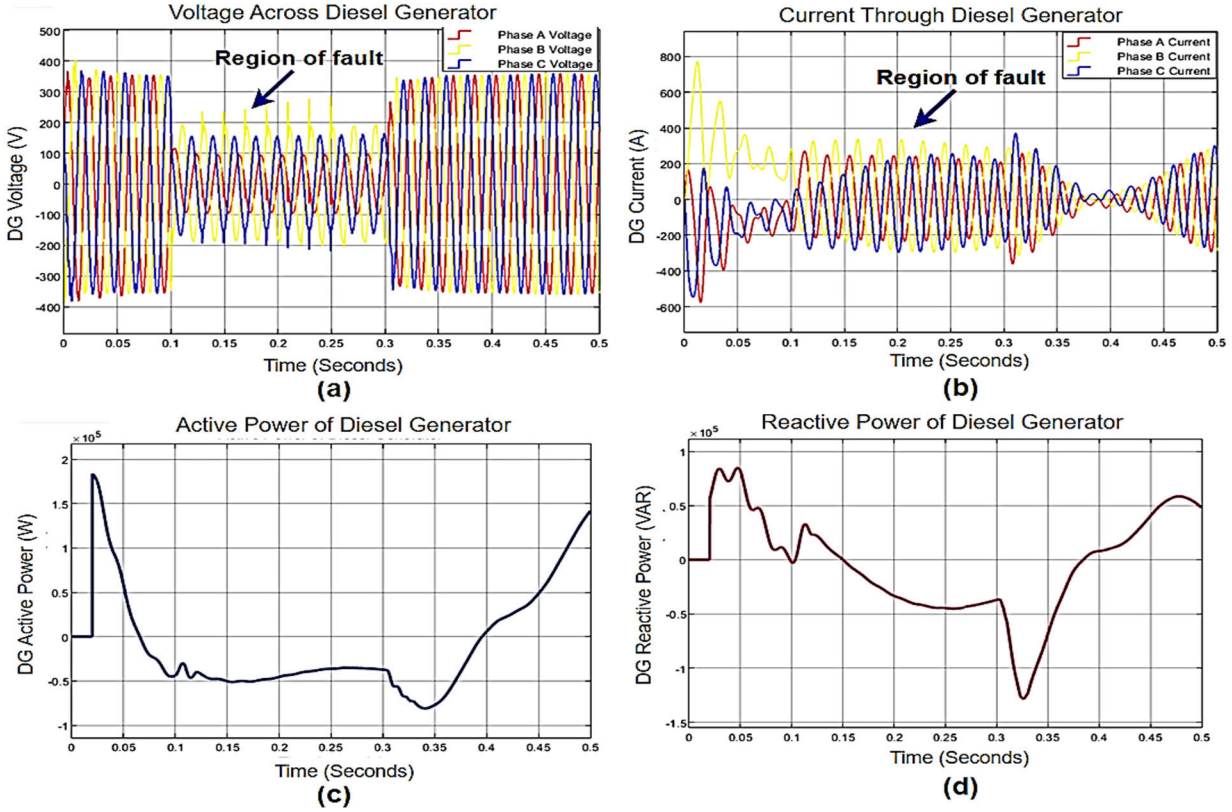

FIGURE 26. DG output plots. (a) Voltage across DG, (b) Current through DG, (c) Active power of DG, (d) Reactive power of DG.

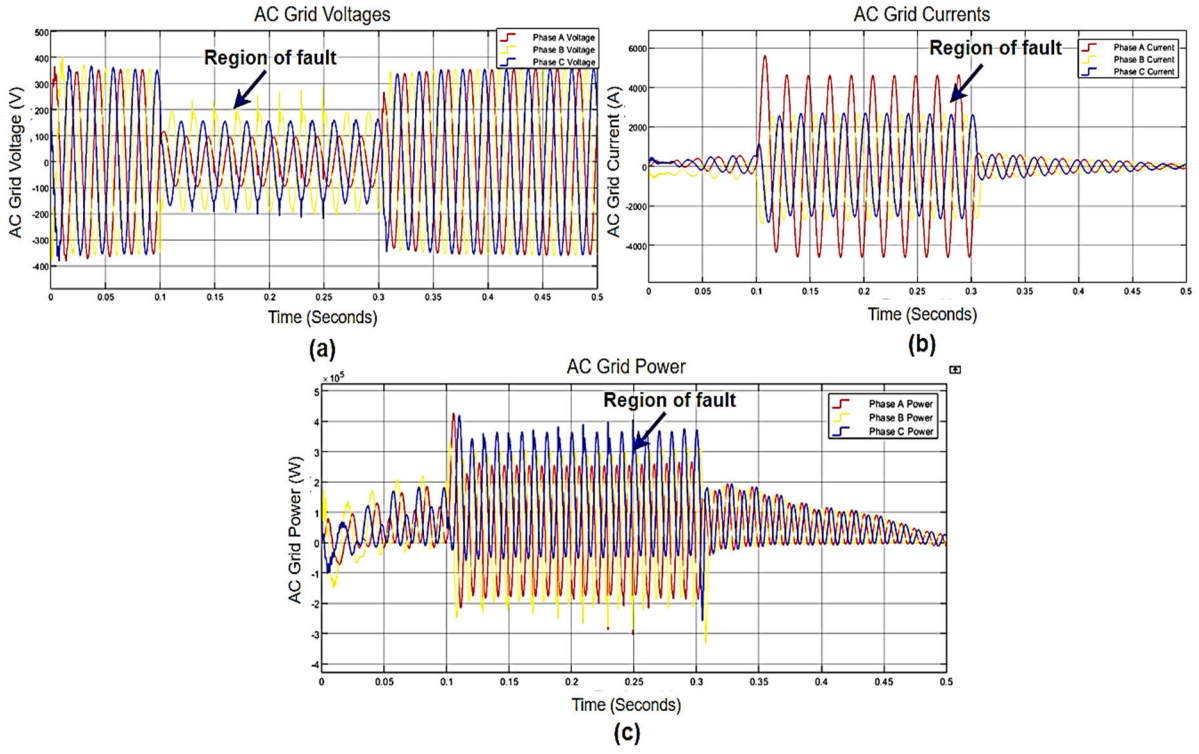

FIGURE 27. AC power grid plots. (a) AC grid voltages, (b) AC grid currents, (c) AC grid power.

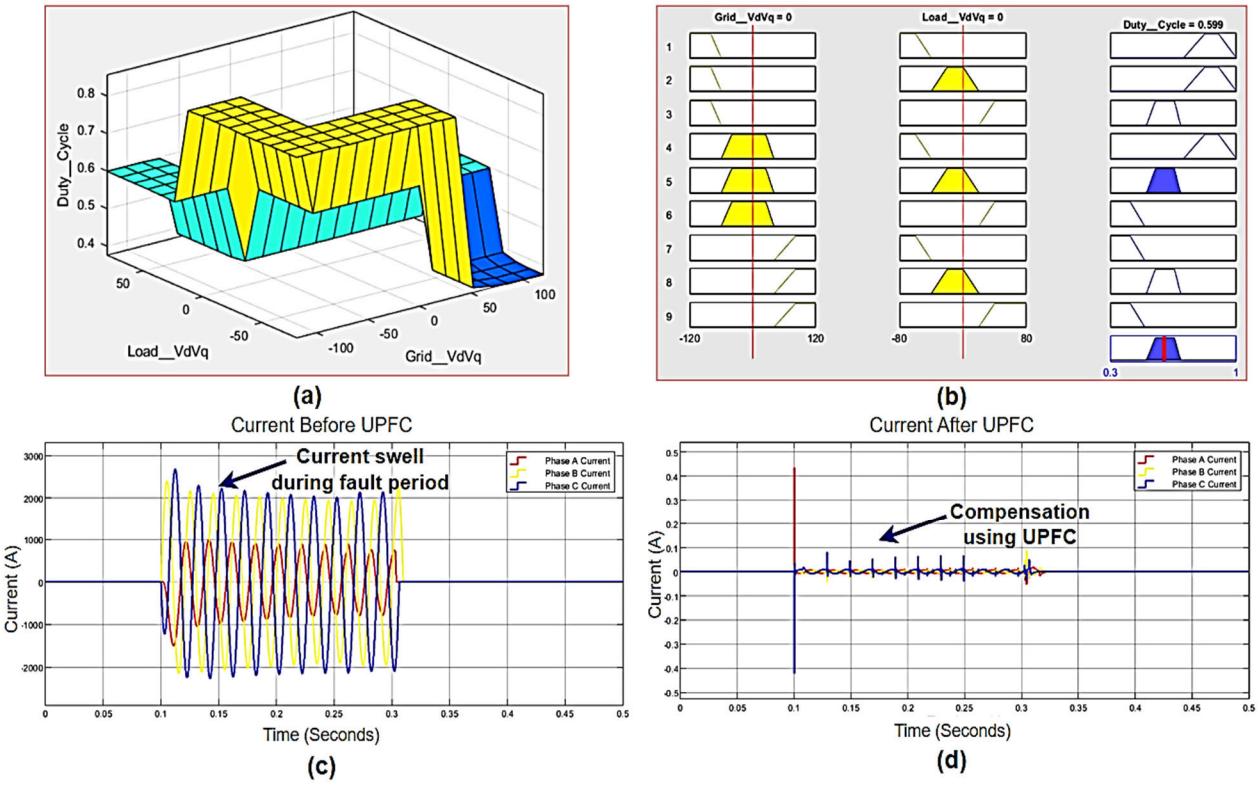

FIGURE 28. Performance analysis of FLC-UPFC plots. (a) FLC surface view of UPFC, (b)FLC fuzzy rule-based output, (c) Current before UPFC, (d) Compensated current after UPFC.

voltage and current graphs depicted in Fig. 23 (a) and (b), it is evident that the battery may be efficiently regulated during the charging and discharging processes. Furthermore, the SoC is efficiently controlled within the range of 99.2% to 100%, as depicted in Fig. 23 (c). Hence, the findings demonstrate that the suggested FLC-based intelligent controller can accurately detect faults and effectively compensate for BESS, BMS, and bidirectional converter performance. As a result, the system's stability is also enhanced.

D. PERFORMANCE ANALYSIS OF VSI PLOTS

The VSI transforms the output from the SPV system and BESS into AC power, enabling its transmission to the grid. The performance graphs of VSI with a fault period from 0.1 to 03 seconds in the proposed work are depicted in Fig. 24. Fig. 24 (a) illustrates the three-phase voltage acquired from the voltage source converter. The plot demonstrates that the three phases consistently generate around 400 V for the whole duration, except the fault period. The VSI voltage is impacted by a grid fault, resulting in a voltage dip in the plot. The VSI controller and the proposed UPFC can effectively regulate the inverter voltage within a defined range, even during a problematic time. The current through the VSI is depicted in Fig. 24 (b). The recorded current is constant, except for a defective period characterised by spikes. Both the controller and UPFC successfully regulated the current to a significant range. Fig. 24 (c) illustrates the active power of the VSI, which is efficiently regulated except instances during fault occurrences. The analysis of the reactive power of VSI is depicted in Fig. 2 (d), illustrating a similar method. The plot demonstrates a strong performance in the conversion of solar as well as battery energy into AC power for integration into the grid. The plots indicate that, despite grid faults leading to voltage dips and current fluctuations, the controller and UPFC effectively uphold stability and regulate the VSI output within acceptable thresholds for most of the operational period.

E. PERFORMANCE ANALYSIS OF DIESEL GENERATOR PLOTS

The DG plays a crucial role in various PS, providing reliable backup power in grid instability. A 30-KVA synchronous generator fuels the DG system under consideration. The frequency of the AC voltage generated is influenced by the mechanical rotor speed of DG, as depicted in Fig. 25 (a), expressed in pu, which is typically modified to align with the grid's frequency or comply with system requirements. The primary function of the DG governor is to regulate the rotational velocity of the generator through the regulation of the DG's speed.

Fig. 25 (b) illustrates the mechanical power production pu of the DG. During the initial phase of the narrative, spanning

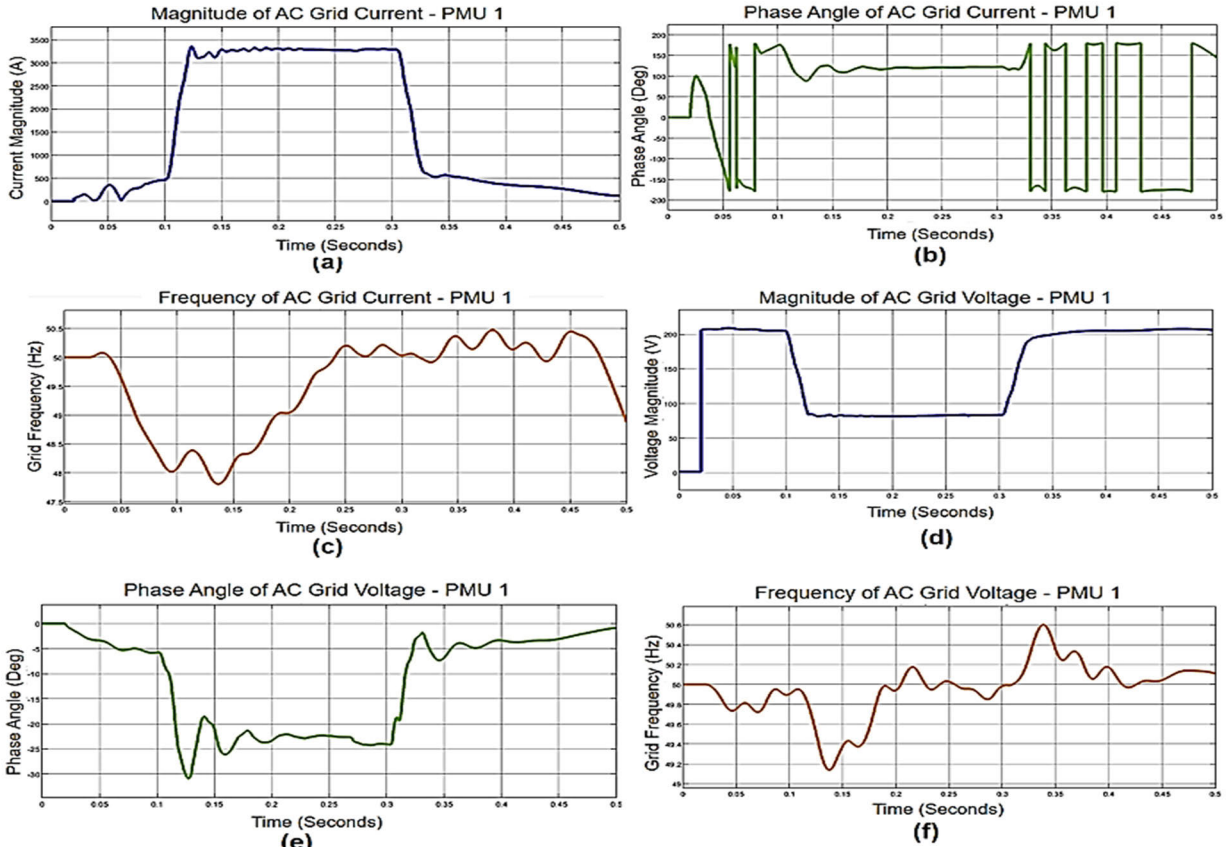

FIGURE 29. Performance evaluation plots for grid PMU. (a) Magnitude of AC grid current, (b) Phase angle of AC grid current, (c) Frequency of AC grid current, (d) Magnitude of AC grid voltage, (e) Phase angle of AC grid voltage, (f) Frequency of AC grid voltage.

from 0 seconds to around 0.03 seconds, the mechanical power of the generator remains in a condition of halt or idle operation. At 0.03 seconds, a rapid surge in mechanical power occurs, culminating in a value of 1 pu and persisting until 0.1 seconds. The rapid increase in power output indicates that the DG is effectively and promptly meeting the load demand. The fault scenario occurs within the time interval of 0.1 to 0.3 seconds, resulting in a subsequent decrease in power that endures for up to 0.16 seconds. This timeframe is most likely required for protective relays to separate the DG from the microgrid because of the fault, guaranteeing the system's stability and avoiding possible harm. After this period of downtime caused by a failure, the DG undergoes another surge in mechanical power at 0.16 seconds. The observed increase in power may indicate the DG's attempt to restore synchronisation with the microgrid or mitigate load fluctuations following the resolution of the incident.

Nevertheless, it rapidly reverts to 0 pu at 0.21 seconds, indicating that the power grid may not be adequately prepared to accommodate the DG's output or necessitate additional stabilisation measures. The extended duration of power deprivation, lasting up to 0.41 seconds, may suggest the ongoing detachment of the generator from the microgrid, potentially as a component of post-fault restoration or synchronisation protocols. At 0.41 seconds, a significant increase in mechanical power is observed, reaching a value of 1.1 pu. The sudden surge in power generation may suggest the effective reintegration of the DG into the microgrid after the fault has been resolved. The generator effectively responds to the system's restored demand and stabilises grid frequency and voltage levels. Fig. 25 (c) illustrates the terminal voltage in pu, revealing a consistent terminal voltage, except for the fault period ranging from 0.1 to 0.3 seconds.

Fig. 26 illustrates the voltage across the DG linked to the grid bus. Fig. 26 (a) depicts the voltage of the DG, with particular emphasis on the fault region. The voltage remains nearly constant at approximately 400 V, except for the fault region between 0.1 and 0.3 seconds. Fig. 26 (b) illustrates the fluctuation of current originating from the DG. Fig. 26 (c) and (d) display both the active and reactive power. It is evident from the plots that the DG efficiently generates power.

F. PERFORMANCE ANALYSIS OF AC POWER GRID PLOTS

Fig. 27 exhibits the AC power grid charts. Fig. 27 (a) illustrates the grid voltages, which show stability at 400 V, except the 3-phase L-G fault occurring within the time interval of 0.1 seconds to 0.3 seconds. The grid current depicted in Fig. 27 (b) exhibits an increase in current during the L-G fault period. Fig. 27 (c) displays the power output of the AC power

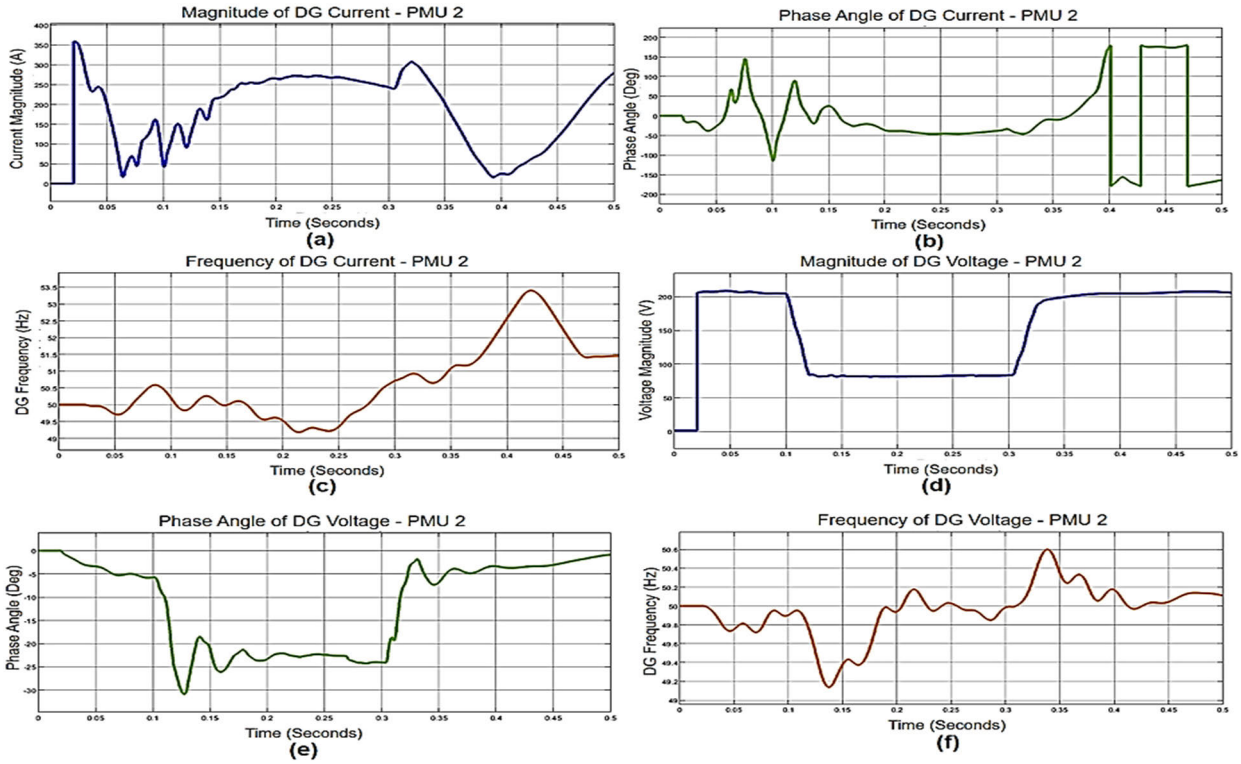

FIGURE 30. Performance evaluation plots for diesel generator bus PMU. (a) Magnitude of DG current, (b) Phase angle of DG current, (c) Frequency of DG current, (d) Magnitude of DG voltage, (e) Phase angle of DG voltage, (f) Frequency of DG voltage.

grid. It is evident from the plot that the system is producing efficient power and capable of meeting the load needs, except for the fluctuations observed during the fault period.

G. PERFORMANCE ANALYSIS OF FLC-BASED UPFC PLOTS

Fig. 28 can be used to assess the efficacy of the proposed FLC-based UPFC. The surface view and fuzzy rule viewer output of the proposed FLC-based UPFC are depicted in Figs.28 (a) and (b). The current swell caused by the L-G fault phase preceding UPFC is illustrated in Fig. 28 (c). Fig. 28 (d) demonstrates that the suggested UPFC efficiently compensates for the current during the fault period (0.1-0.3 sec), resulting in effective power management and compensation in the microgrid utilising the proposed intelligent technique. Consequently, the system's total power quality is enhanced.

H. PERFORMANCE ANALYSIS OF PMU PLOTS

The work utilises four PMUs, with the initial PMU positioned in the AC power grid bus, the second PMU in the DG bus, the third PMU in the SPV-BMS-inverter bus, and the fourth PMU in the load side bus. PMUs are employed to monitor and measure voltages, currents, phase angles, and frequencies accurately, which facilitates the identification of anomalies and deficiencies at a higher accuracy level, guaranteeing the system's stability.

The PMU implemented in the power grid is depicted in Fig. 29. Based on the analysis of Figs. 29 (a) and (d), it is evident that the voltages and currents exhibit a consistent pattern, except for the L-G fault, which manifests within the time interval of 0.1 to 0.3 seconds. By effectively monitoring the PMU data, the defect can be accurately diagnosed, and appropriate corrective steps can be taken. The voltage and current phase angles function effectively, except for anomalies, as depicted in Figs.29 (b) and (e). The utilisation of PMUs for phase angle detection in microgrids is of utmost importance in monitoring and regulating the grid's stability and dependability. PMUs accurately synchronise the voltage and current phasors at different places in the grid. PMUs accurately identify deviations from the optimum operating parameters throughout the fault period (0.1 – 0.3 seconds) that cause instability by analysing the phase angles of these phasors. Operators can utilise this real-time monitoring feature to proactively address the defect by modifying power flows, operating protective relays, or performing corrective operations. This ensures grid stability and prevents the occurrence of cascade failures. Moreover, the phase angle data obtained from PMUs is utilised for extensive monitoring, control, and safety purposes, enabling improved coordination among various grid components, and enhancing the overall resilience and reliability of the system. Figs. 29 (c) and (f) depict the grid voltage and current frequency, respectively. The plots demonstrate effective monitoring of frequencies, including observing frequency changes during fault periods and successfully tracking frequency restoration.

The plots obtained from the PMU installed in the DG bus are depicted in Fig. 30. Like the scenario in Fig. 29, the

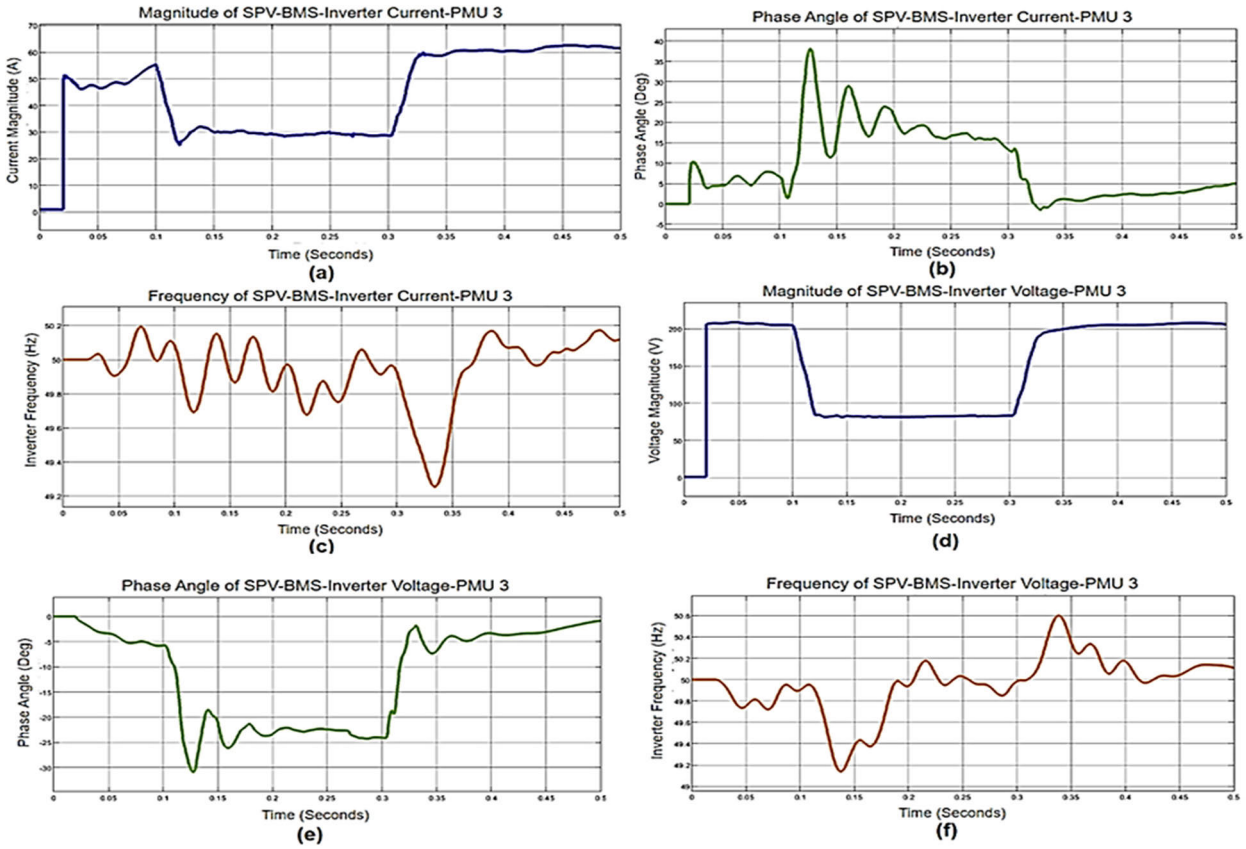

FIGURE 31. Performance evaluation plots for inverter bus PMU. (a) Magnitude of inverter current, (b) Phase angle of inverter current, (c) Frequency of inverter current, (d) Magnitude of inverter voltage, (e) Phase angle of inverter voltage, (f) Frequency of inverter.

PMU proficiently assesses and monitors the magnitudes of voltage and current in the DG and their phase angles and frequencies. Observations are made on deviations within the 0.1 – 0.3 seconds fault period. The plots acquired in the PMU inserted in the inverter bus are depicted in Fig. 31. The PMU can also accurately measure and monitor the voltage, current, phase angles, and frequency variations of the inverter. Fig. 32 displays the PMU graphs acquired from the load bus. The system's efficacy is successfully assessed and monitored in both stable and faulty conditions through a PMU.

IV. ANALYSIS OF SIMULATION RESULTS

The analysis is conducted using the plots derived from the simulation results.

- The SPV system exhibits effective voltage and current generation following fluctuating irradiance levels, thereby highlighting its capacity to adjust to alterations in the surrounding environment. The direct correlation between current and voltage fluctuations and irradiation changes underscores the system's responsiveness. The power curve demonstrates the adequacy of power generation in microgrid applications, guaranteeing a sufficient energy supply.
- The proposed FLC in SPV-based boost converter efficiently controls the MPPT operation, guaranteeing optimal power efficiency of the SPV system. The management of voltage and current fluctuations is conducted within acceptable parameters, ensuring the maintenance of optimal power generation in the face of environmental and load fluctuations. The power output consistently remains near the MPP, augmenting the overall efficiency of energy conversion.
- The suggested FLC enables effective regulation of the bidirectional converter and BESS, guaranteeing consistent performance in regular and faulty circumstances. FLC immediately mitigates voltage and current variations during disturbances, ensuring system stability. The battery's SoC is efficiently regulated to maintain desirable thresholds, facilitating optimal charging and discharging.
- The VSI effectively converts the outputs of SPV and BESS into AC electricity for integration into the grid. The VSI controller and UPFC effectively regulate voltage and current, maintaining grid stability even in grid disturbances. The stability of active and reactive power production is crucial in facilitating efficient power supply to the grid.

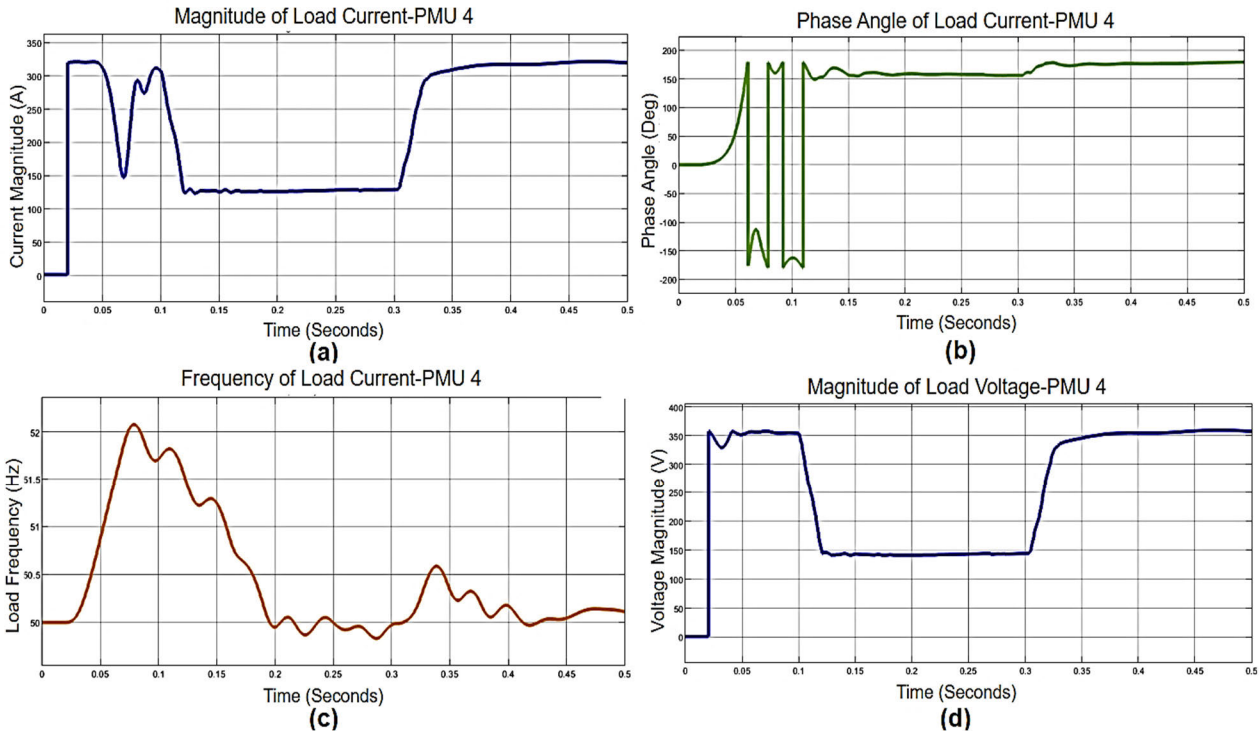

FIGURE 32. Performance evaluation plots for load bus PMU. (a) Magnitude of load current, (b) Phase angle of load current, (c) Frequency of load current, (d) Magnitude of load voltage, (e) Phase angle of load voltage, (f) Frequency of load voltage.

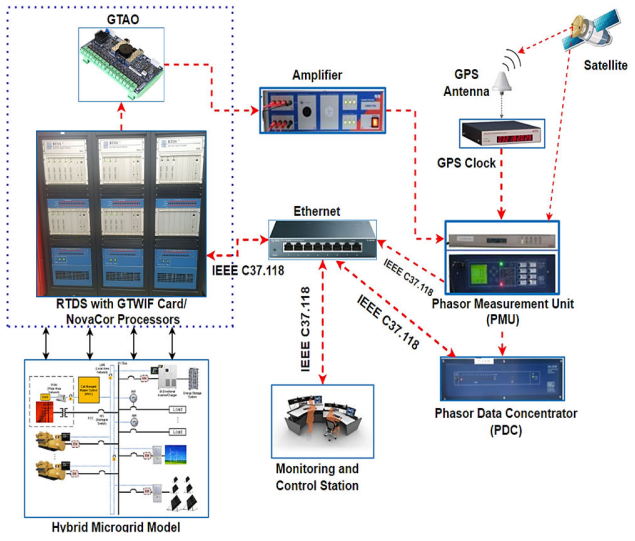

FIGURE 33. RTDS for WAMS using hardware PMU.

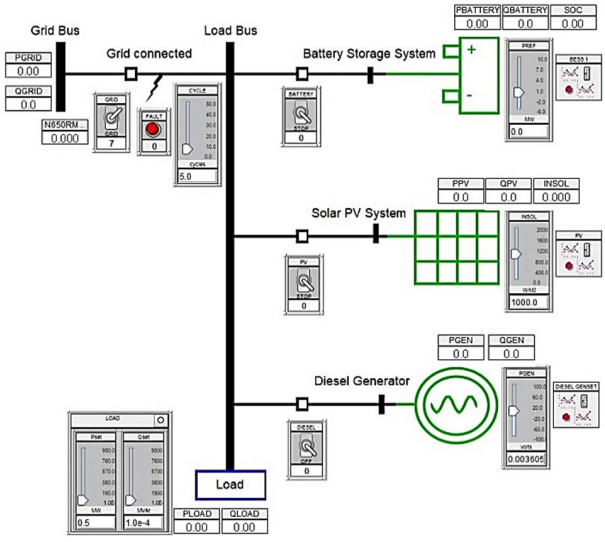

FIGURE 34. Single-line diagram of proposed microgrid for RTDS.

- The DG system installed to the grid efficiently addresses grid instability by providing backup power during failures. The mechanical power generation corresponds to the load requirements, demonstrating the dependability of DG. The voltage and current of the AC power grid stay constant, except during fault periods, which suggests that the system is functioning effectively. Under typical circumstances, the AC power grid demonstrates stable current, voltage, and power production. However, there are variations in current flow in fault occurrences, while the total power generation remains optimal.
- The utilisation of FLC-based UPFC mitigates current fluctuations that occur during fault periods, facilitating efficient power management and maintaining grid stability. UPFC's sophisticated adjustment technique improves the overall power quality of the system.

TABLE 15. Design paramters of RTDS using RSCAD.

Parameters	Values
AC Source	
Voltage input time constant	0.05 Sec
Series resistance	1*e-3 Ω
Parallel resistance	1 Ω
Parallel inductance	0.1 H
RMS value of initial source (magnitude)	0.48 kV
Frequency	50 Hz
Load flow result of real power	-0.000657 MW
Load flow result of reactive power	-0.038771 MVAR
Source voltage during Fault	0.50 pu
Bus Data	
Bus type	Slack
Voltage from load flow	1 pu
Bus type	PQ bus
Voltage from load flow	1 pu
Fault	
Fault type	L-G
Fault duration	0.10 Sec
A, B and C phase ground fault resistances	1*e-6 Ω
Load	
Type of load	RL
Rated L-L bus voltage (RMS)	0.48 kV
Minimum bus voltage (L-L)	0.5 pu
Active power (initial)	0.3 MW
Minimum active power, maximum active power	0.0001 MW, 1000 MW
Reactive power (initial)	0.0001 MVAR
Minimum reactive power, maximum reactive power	0.0001 MVAR, 10000 MVAR
SPV System	
Initial irradiance	1000 W/m2
Final irradiance	2000 W/m2
Minimum irradiance	0 W/m2
Initial temperature	25 Deg C
Maximum temperature	80 Deg C
Minimum temperature	-80 Deg C
Model of SPV	Single diode five-parameter model
MPPT technique	Lambert function approximation method
Number of series connected cells/ string/module	36 Nos
Parallel cell string number	1 No
Voltage at open circuit	21.7 V
Current when short circuit	3.35 A
Voltage when power is maximum	17.4 V
Current when power is maximum	3.05 A
Number of modules when connected in series	115 Nos
Number of modules when connected in parallel	66 Nos
SPV Controller	
Filter resistance (AC side)	2*e-3 Ω
Filter inductance (AC side)	100*e-6 H
Series resistance (DC side)	1*e-6 Ω
Filter capacitance (DC side)	5000 µF
Injection resistance (DC side)	2*e3 Ω
Diesel Generator	
DG base angular frequency	50 Hz
The initial terminal voltage of the excitation system	1 pu
Voltage regulator gain of excitation system	200 pu
Voltage regulator time constant of exciter	0.4 sec
Rated MVA of the machine	1.25 MVA
Rates RMS L-L voltage	0.48 kV
The inertia constant of the generator	1.7 MWs/MVA
Stator leakage reactance	0.130 pu
Stator resistance	0.002 pu
Battery Energy Storage System (BESS)	
Battery type	Li-Ion
Number of cells of battery in series in one stack	250 EA
Number of cells of battery in parallel in one stack	250 EA
Single-cell capacity	0.85 Ah
% SoC (initial) in a single-cell	85%
AC side filter resistance of BESS control	2*e-3 Ω
AC side filter inductance of BESS control	100*e-6 H
Series resistance (DC side)	0.001 Ω
Filter capacitance (DC side)	5000 µF
Injection resistance (DC side)	2*e3 Ω
Phasor Measurement Unit (PMU)	
Data communication channel used in GTNET	C37.118
Base frequency	50 hz
Number of PMU	1 No
Reporting rate	30 frames/sec

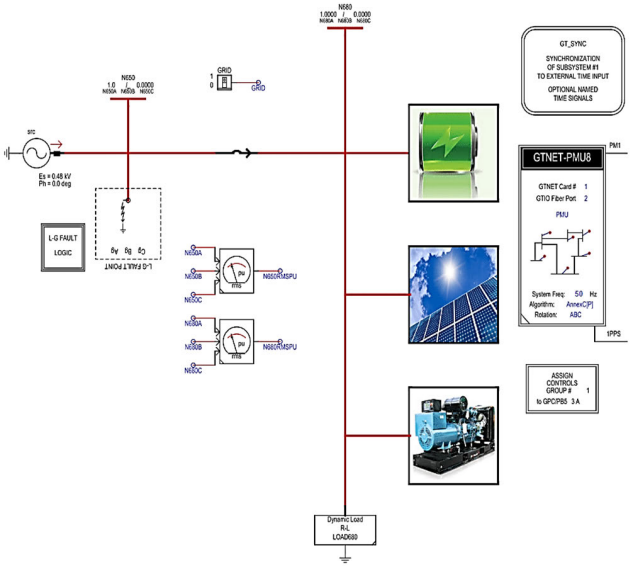

FIGURE 35. PMU layout of the proposed microgrid using RSCAD.

- PMUs offer precise monitoring and the measurement of diverse grid characteristics, enabling the identification of faults and implementation of corrective measures. The effective tracking of currents, voltages, phase angles, and frequencies can achieve the proactive control of faults and enhance grid resilience.

So, it is evident from the results that the combination of intelligent-based FLCs, PMUs, and effective control methods successfully improves fault detection, compensation, and power management in microgrids. This ensures the system operates reliably and consistently, even in challenging conditions.

V. RTDS VALIDATION USING RSCAD

To verify the accuracy of the work performed in this study using MATLAB/Simulink, the identical system is simulated using RSCAD and subjected to RTDS. The resulting plots are assessed by including a PMU in the system. Using ST in the RTDS of Wide Area Monitoring Systems (WAMS)

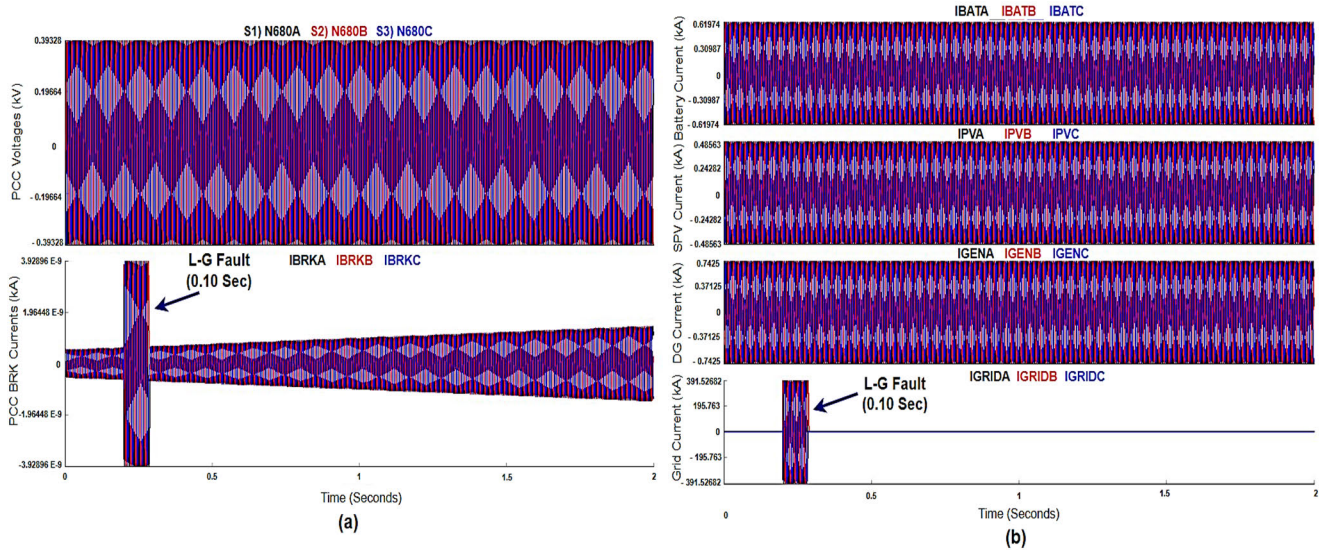

FIGURE 36. RTDS output plots of the proposed microgrid a) PCC voltages and PCC breaker currents during fault, b) Current plots of battery, SPV system, diesel generator and Grid Current.

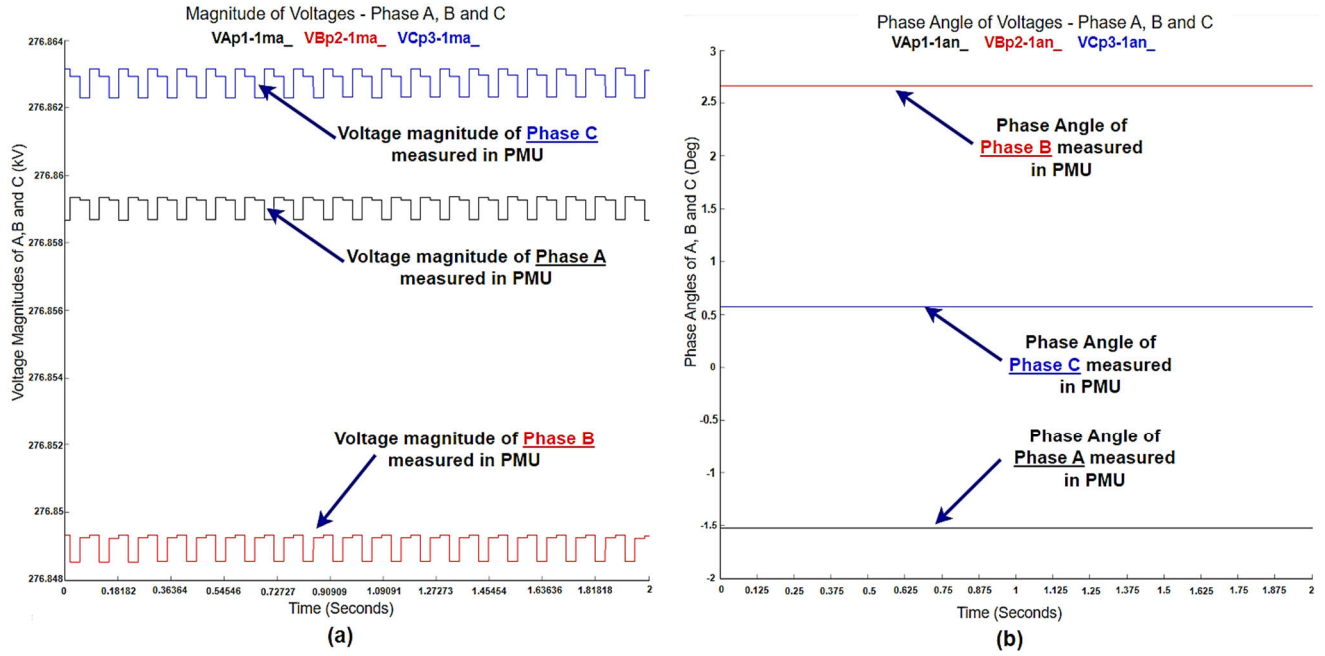

FIGURE 37. Magnitude of voltages and phase angles of phases A, B and C measured in PMU using RTDS.

has emerged as an innovative method for improving grid monitoring and control capabilities. WAMS utilises PMUs to include them in PS. This integration allows for collecting real-time, high-resolution information regarding grid conditions. This data empowers operators to make prompt and well-informed decisions to ensure stability, enhance dependability, and optimise grid performance. The utilisation of this technology presents numerous benefits, such as heightened situational awareness, more significant fault detection, localization capabilities, improved power system visualisation, and facilitation of advanced control and safeguarding techniques. WAMS plays a vital role in contemporary power system management because of its wide-ranging applications, which encompass wide-area monitoring and control, oscillation detection, dynamic stability assessment, and post-event analysis. There are two types of RTDS for WAMS: one that utilises software PMUs while the other that utilises hardware PMUs.

Fig. 33 depicts the RTDS for WAMS, which integrates hardware-based PMUs to improve the precision and dependability of measurements, which is the methodology proposed in this work. The system incorporates satellite-based time synchronization, GPS clock and an RTDS platform equipped with a GTWIF Card/NovaCor processor.

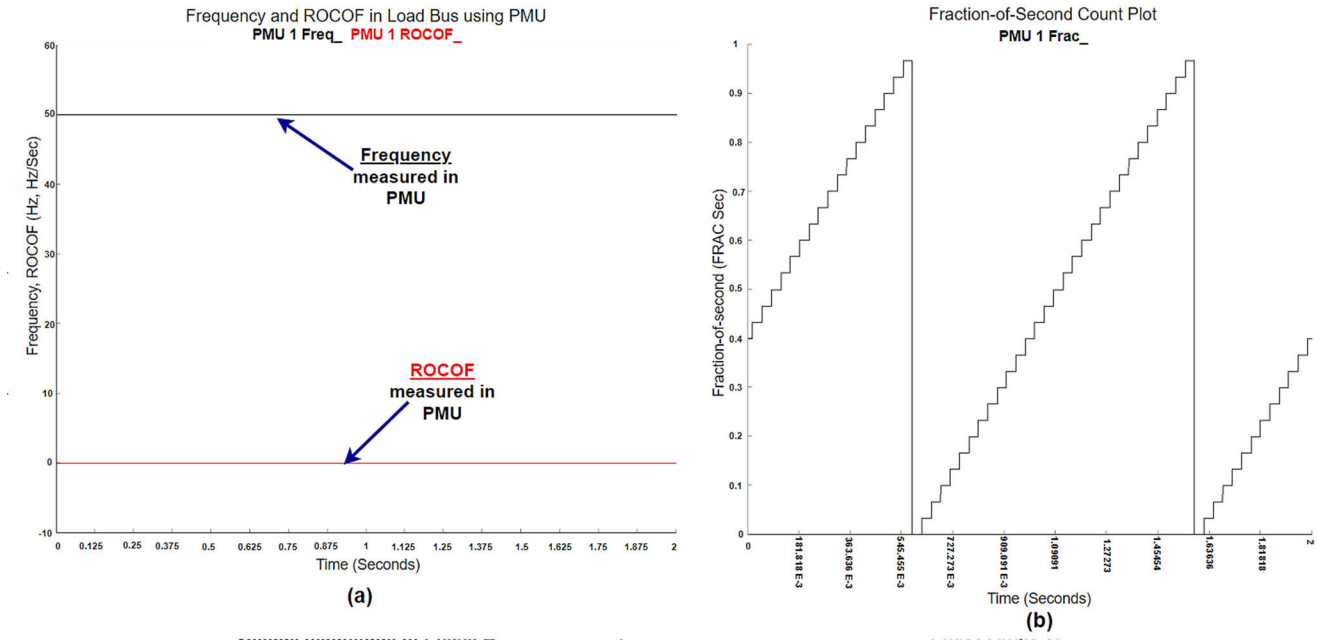

FIGURE 38. Frequency, ROCOF and fraction-of-second count plots measured in PMU using RTDS.

In this arrangement, PMUs directly assess synchrophasors, circumventing the necessity for software emulation. Before data capture, the GTAO and amplifier modules guarantee precise signal conditioning and amplification. Data transmission to the PDC is facilitated through ethernet connections, following the IEEE C37.118 standards. The control station is responsible for processing, analysing, and visualising real-time synchrophasor data to enhance grid monitoring and control activities. Using hardware PMUs in this configuration provides enhanced measurement accuracy, facilitating more detailed grid analysis and more dependable decision-making in crucial operating situations. The suggested study employs this RTDS configuration and conducts the simulation using RSCAD.

Fig. 34 depicts the single-line diagram of the microgrid for RTDS with the identical components selected in the MATLAB/Simulink software. An SPV system, in addition to a BESS and a DG, is implemented and linked to the load bus. A grid bus is linked to the load bus. A three-phase fault is created between the load bus and the grid bus. To ensure efficient monitoring and measurement of the system's parameters, anomaly detection and performance, a PMU is incorporated into the system to leverage the ST. Fig. 35 shows the system layout after the PMU is connected to the proposed microgrid. The selected parameters for the system design in RTDS using RSCAD are provided below in Table 15.

Fig. 36 displays the plots generated by the RTDS, including a hardware-based PMU. Fig. 36 (a) shows the voltage at the Point of Common Coupling (PCC) and the current flowing through the PCC breaker during an L-G fault. This fault lasts for 0.10 seconds in real-time. The PCC voltage plot indicates that the three phases, A, B, and C, steadily increase and are measured at a peak value of 392.8 V. From the PCC breaker current plot, it is evident that a significant increase in current, reaching a value of 3.92896*E-9 kA, occurs during the fault period. The installed PMU efficiently monitors and measures the fault in real-time.

Fig. 36 (b) depicts the currents of the battery, SPV system, and grid when the SPV, BESS, and DG are activated, providing power to the grid to fulfil the load demands. The battery current is accumulated and measured at a peak-peak value of 0.61974 kA, whereas the SPV current is measured at a peak-peak value of 0.48563 kA and the DG current with a peak-peak value of 0.7425 kA. The PMU efficiently monitors the grid current during a fault state in real-time and measures it as 391.52682 kA during the fault duration.

The IEEE C37.118 standard guarantees the interoperability and dependability of data transmission for the microgrid. In addition, the PMU that relies on hardware can promptly and precisely identify defects, hence facilitating prompt compensation and management measures. After a fault occurs, both current and voltage are regulated, demonstrating the efficiency of the fault-compensating mechanisms. During faults, the SPV and BESS systems will decrease output, while the DG increases its power output to compensate for the shortfall.

The PMU offers accurate measurements of voltage magnitudes and associated phase angles for the three phases, as depicted in Fig. 37. The values provided are real-time information that allows for immediate monitoring and control and is essential for detecting faults and managing electricity in the microgrids being suggested. In a balanced three-phase system, the voltage magnitude should be uniform and have equal magnitudes, along with a 120-degree phase shift. Any variation indicates the presence of possible problems, such as phase abnormalities or faults. The PMU efficiently measures

TABLE 16. Comparison of proposed work with previously published works in literature.

Aspect	Proposed System	Existing Systems	References
Real-time monitoring	Utilizes ST-enabled PMUs for real-time grid monitoring and management, providing higher accuracy and proactive control.	Most systems depend on SCADA, which lacks precise real-time monitoring for periodic data collection.	[24], [25], [26], [27]
Simulation and validation	The system is simulated in MATLAB/Simulink and is validated using RTDS with RSCAD incorporating hardware-based PMUs for precise real-time measurements.	Studies only rely on MATLAB/Simulink and comparison without comprehensive real-time validation in varying conditions.	[9], [15], [24], [29], [31], [39]
FLC-based intelligent controllers	Integration of FLCs in SPV-based MPPT, BESS and UPFC will help improve the proposed microgrid's effectiveness, ensuring improved power quality, voltage regulation, grid stability and the grid's ability to withstand internal faults and varying power demand.	Using traditional and a combination of conventional and intelligent-based controllers will affect voltage regulation and system stability, especially in the varying nature of RES in microgrids.	[6], [9], [15], [19], [20], [33], [45]
Fault detection and compensation	Fast and effective detection using ST-enabled PMUs and improved fault compensation using FLC-based UPFC.	Limited fault detection capabilities and slower response using traditional SCADA systems and controllers.	[24], [25], [26], [27]
Power management	Effective power management can be achieved by using proposed FLCs in SPV-BESS-DG-based microgrids where solar irradiance varies in nature. Also, PMUs detect the grid anomalies effectively to take control action faster.	Power management is moderate due to the intermittent solar irradiance anomaly detection during faults using SCADA systems.	[5], [14], [15], [24], [25], [26]
Power blackouts and cybersecurity in PS	PMU-enabled PS can effectively monitor and measure the anomalies and cybersecurity issues presented in the PS network and take remedial actions by switching the converters and intelligent-based FLC controllers.	SCADA systems and traditional controllers fail to identify the transient changes and anomalies in the PS network, leading to PS blackouts.	[9], [15], [19], [24], [25], [26], [27]
Cost, installation and maintenance	Higher installation cost (FLCs-PMUs-UPFC), followed by complex installation and maintenance, but provides advanced monitoring with PMUs.	Moderate or higher costs based on the controllers, SCADA systems, FACTS devices (SVC, STATCOM, TCSC), and moderate installation and maintenance are also available.	[15], [16], [19], [21], [22], [23], [27]

the magnitudes of phases A, B, and C from Fig. 37 (a) and plots the appropriate phase angles in Fig. 37 (b). Given the stable output of the PCC voltage in Fig. 36 (a), the magnitudes and phases associated with it likewise exhibit stability.

Fig. 38 displays the frequency, ROCOF, and fraction-of-second plot acquired from the PMU, which are crucial for evaluating the microgrid's stability. Fig. 38 (a) demonstrates that the frequency remains consistently at a nominal value of 50 Hz, while the ROCOF plot confirms its efficacy. High ROCOF values indicate rapid and abrupt fluctuations in frequency, commonly linked to faults or sudden variations in load. However, in this case, the ROCOF is maintained at zero for the entire duration.

Fig. 38 (b) displays the plot of the count of fractions of a second acquired from PMU observations in a microgrid. These measurements utilise the exact time-stamping ability of ST using PMU, enabling accurate synchronisation and coordination of events throughout the microgrid. The level of detail is essential for identifying and examining temporary occurrences with high time precision, such as malfunctions or abrupt shifts in load. Through thorough analysis, the precise timing and order of events can be obtained, leading to improved identification of faults, isolation of issues, and enhanced system stability, all in real-time. This level of specificity facilitates improved decision-making and optimisation of microgrid effectiveness, ultimately enhancing dependability and efficiency.

Testing the proposed system utilising RTDS and RSCAD, in addition to hardware-based PMUs, showcases the system's capacity to identify and rectify defects accurately. An in-depth examination of the plots yields crucial observations on the microgrid's effectiveness and stability, guaranteeing the suggested system's dependable functioning.

VI. NOVELTY ASSESSMENT OF THE PROPOSED SYSTEM WITH EXISTING SYSTEMS

The uniqueness of the proposed system can be assessed by comparing it to previously published studies cited in the literature. The comparison is conducted in Table 16.

VII. CONCLUSION AND FUTURE SCOPE

The authors suggested an intelligent-based fault detection, compensation, and power management approach for microgrids employing FLCs and PMUs. The system showcased resilience in adjusting to variable environmental conditions and load fluctuations by incorporating SPV systems, DG, BESS, VSI and UPFC with the help of proposed FL-based controllers. The examination of the SPV system demonstrated its ability to effectively produce current and voltage following different irradiance levels, guaranteeing a steady power supply inside the microgrid. Furthermore, the control strategies adopted using FLCs in MPPT-based SPV systems, BMS and UPFC effectively regulated power generation and storage, ensuring optimal performance in normal and fault conditions. Also, ST-utilising PMUs, installed in the buses on the grid side, DG, inverter, and load, enable accurate measurement, monitoring, and detection of anomalies occurring during fault periods. Therefore, the suggested system guarantees reliable and consistent operation, even under challenging circumstances.

Moreover, the suggested system's dependability and effectiveness were verified by utilising RTDS with PMUs in real-world settings. By utilising hardware-based PMUs, the system can precisely monitor grid interactions in real-time, allowing for the timely identification of disruptions and proactive implementation of control measures. The RTDS simulations demonstrated the system's capacity to uphold grid stability and effectively handle faults, as indicated by the accurate voltage and current magnitudes, their phase angles, frequency, and ROCOF in fault scenarios. Finally, the novelty of the suggested system is analysed by comparing the results obtained with those of the existing literature. In short, integrating intelligent FLCs, PMUs, and advanced control techniques has shown substantial enhancements in microgrids' fault identification, compensation, and power management, guaranteeing dependable and consistent operation, even in challenging situations. The following future endeavours can expand upon the research conducted.

- Improved fault identification and compensation can be accomplished by implementing sophisticated fault/anomaly detection algorithms utilising modern Machine Learning (ML) techniques like neural networks or deep learning.
- Advanced power management techniques, such as particle swarm optimisation, model predictive control, and genetic algorithms, can manage energy in real-time considering dynamic pricing, response to demand, and energy storage.
- Incorporating advanced technologies like PMUs into the Internet of Things to enable instantaneous monitoring and control.
- Synchronized control systems can be implemented in PMUs utilizing advanced communication technologies like 5G and 6G and blockchain for secure and distributed control.

LIST OF ACRONYMS

BC	– Battery Charging.
BD	– Battery Discharging.
BESS	– Battery Energy Storage System.
BMS	– Battery Management System.
CTs	– Current Transformers.
DERs	– Distributed Energy Resources.
DG	– Diesel Generator.
DSTATCOM	– Distributed Static Compensators.
FACTS	– Flexible AC Transmission System.
FL	– Fuzzy Logic.
FLC	– Fuzzy Logic Controller.
MPPT	– Maximum Power Point Tracking.
NPIV	– Negative Peak Inverse Voltage.
PCC	– Point of Common Coupling.
P&O	– Perturb and Observe.
PDC	– Phasor Data Collector/Concentrator.
PMU	– Phasor Measurement Units.
PS	– Power Systems.
PTs	– Potential Transformers.
PWM	– Pulse Width Modulation.
RES	– Renewable Energy Sources.
ROCOF	– Rate of Change of Frequency.
RTDS	– Real-Time Digital Simulator.
SCADA	– Supervisory Control and Data Acquisition System.
SESS	– Smart Energy Storage System.
SoC	– State of Charge.
SPV	– Solar Photovoltaic.
SSSC	– Static Synchronous Series Compensator.
ST	– Synchrophasor Technology.
STATCOM	– Static Compensator.
SVC	– Static Var Compensators.
THD	– Total Harmonic Distortion.
UPFC	– Unified Power Flow Controller.
VSC	– Voltage Source Converter.
VSI	– Voltage Source Inverter.
WAMS	– Wide Area Monitoring Systems.
WECS	– Wind Energy Conversion System.

REFERENCES

[1] C. Breyer et al., "On the history and future of 100% renewable energy systems research," *IEEE Access*, vol. 10, pp. 78176–78218, 2022.

[2] R. Wallsgrove, J. Woo, J.-H. Lee, and L. Akiba, "The emerging potential of microgrids in the transition to 100% renewable energy systems," *Energies*, vol. 14, no. 6, p. 1687, Mar. 2021.

[3] N. Karami, N. Moubayed, and R. Outbib, "General review and classification of different MPPT techniques," *Renew. Sustain. Energy Rev.*, vol. 68, pp. 1–18, Feb. 2017.

[4] V. R. Vakacharla, K. Gnana, P. Xuewei, B. L. Narasimaharaju, M. Bhukya, A. Banerjee, R. Sharma, and A. K. Rathore, "State-of-the-art power electronics systems for solar-to-grid integration," *Sol. Energy*, vol. 210, pp. 128–148, Nov. 2020, doi: 10.1016/j.solener.2020.06.105.

[5] S. Singh, V. Narayanan, B. Singh, and B. K. Panigrahi, "Power management with parallel connected voltage source converters for solar photovoltaic battery storage standalone system," in *Proc. IEEE IAS Global Conf. Emerg. Technol. (GlobConET)*, May 2023, pp. 1–6, doi: 10.1109/GlobConET56651.2023.10149928.

[6] A. K. Pandey, V. Singh, and S. Jain, "Maximum power point tracking algorithm based on fuzzy logic control using P-V and I-V characteristics for PV array," *IEEE Trans. Ind. Appl.*, vol. 59, no. 4, pp. 4572–4583, Aug. 2023, doi: 10.1109/TIA.2023.3272536.

[7] R. Liu, G. Zhou, Q. Tian, and G. Xu, "Extendable multiport high step-up DC–DC converter for photovoltaic-battery systems with reduced voltage stress on switches/diodes," *IEEE Trans. Ind. Electron.*, vol. 70, no. 9, pp. 9123–9135, Sep. 2023.

[8] Y. Yang, S. Bremner, C. Menictas, and M. Kay, "Modelling and optimal energy management for battery energy storage systems in renewable energy systems: A review," *Renew. Sustain. Energy Rev.*, vol. 167, Oct. 2022, Art. no. 112671.

[9] M. Barukčić, T. Varga, T. Benšić, and V. J. Štil, "Optimal allocation of renewable energy sources and battery storage systems considering energy management system optimization based on fuzzy inference," *Energies*, vol. 15, no. 19, p. 6884, Sep. 2022.

[10] B. Singh, G. Pathak, and B. K. Panigrahi, "Seamless transfer of renewable-based microgrid between utility grid and diesel generator," *IEEE Trans. Power Electron.*, vol. 33, no. 10, pp. 8427–8437, Oct. 2018.

[11] S. Işçan and O. Arıkan, "Economic operation of a micro grid structured university campus via optimal diesel generator operation under different strategies: A case study," *Electr. Eng.*, pp. 1–22, Feb. 2024, doi: 10.1007/s00202-024-02253-7. [Online]. Available: https://link.springer.com/article/10.1007/s00202-024-02253-7

[12] M. Liaqat, T. Alsuwian, A. A. Amin, M. Adnan, and A. Zulfiqar, "Transient stability enhancement in renewable energy integrated multi-microgrids: A comprehensive and critical analysis," *Meas. Control*, vol. 57, no. 2, pp. 187–207, Feb. 2024.

[13] G. Glanzmann, "FACTS: Flexible alternating current transmission systems," ETH Zürich, Zürich, Switzerland, 2005. [Online]. Available: https://www.research-collection.ethz.ch/handle/20.500.11850/148438
[14] R. Kljajic, P. Marić, F. Relić, and H. Glavaš, "Battery energy storage systems and FACTS devices influence on microgrid voltage stability," in *Proc. Int. Conf. Smart Syst. Technol. (SST)*, Oct. 2020, pp. 141–146.
[15] R. Al Badwawi, W. R. Issa, T. K. Mallick, and M. Abusara, "Supervisory control for power management of an islanded AC microgrid using a frequency signalling-based fuzzy logic controller," *IEEE Trans. Sustain. Energy*, vol. 10, no. 1, pp. 94–104, Jan. 2019.
[16] D. Sarathkumar, A. A. Stonier, and M. Srinivasan, "An extensive critique on FACTS controllers and its utilization in micro grid and smart grid power systems," in *Proc. ICRCCV*, 2023, pp. 323–333.
[17] L. A. Paredes, M. G. Molina, and B. R. Serrano, "Enhancing dynamic voltage stability in resilient microgrids using FACTS devices," *IEEE Access*, vol. 11, pp. 66150–66176, 2023.
[18] I. Marouani, T. Guesmi, B. M. Alshammari, K. Alqunun, A. S. Alshammari, S. Albadran, H. Hadj Abdallah, and S. Rahmani, "Optimized FACTS devices for power system enhancement: Applications and solving methods," *Sustainability*, vol. 15, no. 12, p. 9348, Jun. 2023.
[19] K. Sarita et al., "Power enhancement with grid stabilization of renewable energy-based generation system using UPQC-FLC-EVA technique," *IEEE Access*, vol. 8, pp. 207443–207464, 2020.
[20] M. Osama abed el-Raouf, S. A. A. Mageed, M. M. Salama, M. I. Mosaad, and H. A. AbdelHadi, "Performance enhancement of grid-connected renewable energy systems using UPFC," *Energies*, vol. 16, no. 11, p. 4362, May 2023.
[21] P. K. Pandey and B. Bag, "A comparative study on UPFC and SVC towards voltage profile improvement of a grid connected distributed generation system," in *Proc. Int. Conf. Energy, Power Environment: Towards Sustain. Growth (ICEPE)*, Jun. 2015, pp. 1–5.
[22] M. N. H. Shazon, N.-A. Masood, and H. M. Ahmed, "Modelling and utilisation of frequency responsive TCSC for enhancing the frequency response of a low inertia grid," *Energy Rep.*, vol. 8, pp. 6945–6959, Nov. 2022.
[23] I. N. Muisyo and K. K. Kaberere, "Utilization of FACTS devices in power systems: A review," in *Proc. Sustain. Res. Innov. Conf.*, 2022, pp. 1–7.
[24] M. Dhinu Lal and R. Varadarajan, "Synchrophasor enabled energy monitoring, management and control of solar PV-battery interfaced microgrid," in *Proc. 2nd Int. Conf. Smart Technol. Power Renew. Energy (SPECon)*, Apr. 2024, pp. 1–8, doi: 10.1109/SPECon61254.2024.10537261.
[25] M. D. Lal and R. Varadarajan, "A review of machine learning approaches in synchrophasor technology," *IEEE Access*, vol. 11, pp. 33520–33541, 2023.
[26] M. Tsebia and H. Betarzi, "Improve monitoring system of interconnected oscillation power system based on PMU technology," in *Proc. Int. Conf. Electr. Eng. (ICEE)*, Sep. 2020, pp. 1–6.
[27] A. T. Mathew and M. N. Aravind, "PMU based disturbance analysis and fault localization of a large grid using wavelets and list processing," in *Proc. IEEE Region 10 Conf. (TENCON)*, Nov. 2016, pp. 879–883.
[28] A. Waqar, Z. Khurshid, J. Ahmad, M. Aamir, M. Yaqoob, and I. Alam, "Modeling and simulation of phasor measurement unit (PMU) for early fault detection in interconnected two-area network," in *Proc. 1st Int. Conf. Power, Energy Smart Grid (ICPESG)*, Apr. 2018, pp. 1–6.
[29] R. O. Bawazir, N. S. Çetin, and W. Fadel, "Optimum ground-mounted on-grid connected photovoltaic system," *J. Cleaner Prod.*, vol. 447, Apr. 2024, Art. no. 141294.
[30] R. Sreedhar, K. Karunanithi, and S. Ramesh, "Design, implementation and empirical analysis of a cascaded hybrid MPPT controller for grid tied solar photovoltaic systems under partial shaded conditions," *Meas., Sensors*, vol. 31, Feb. 2024, Art. no. 100961.
[31] B. Vijayakumar, K. S. Rajesh, A. V. P. Kumar, and Y. Ramanjaneyulu, "Optimizing battery charging with a photovoltaic-driven DC–DC boost converter system," *Migration Lett.*, vol. 21, no. S7, pp. 803–818, 2024.
[32] K. Nisha and R. Beniwal, "Comparison of efficiency of various DC–DC converters connected to solar photovoltaic module," *Environ. Sci. Pollut. Res.*, vol. 30, no. 30, pp. 75720–75734, May 2023.
[33] S. S. Raghuwanshi and V. Khare, "FLC based MPPT controller for optimal tracking photovoltaic system," in *Proc. Int. Conf. Inf., Commun., Instrum. Control (ICICIC)*, Aug. 2017, pp. 1–6.
[34] C. Pavithra, S. Vidhyareni, M. Vijayadharshini, K. B. Akshaya, and N. Varsha, "Comparison of solar P&O and FLC-based MPPT controllers & analysis under dynamic conditions," *EAI Endorsed Trans. Energy Web*, vol. 11, pp. 1–6, Jan. 2024. [Online]. Available: https://publications.eai.eu/index.php/ew/article/view/4988
[35] M. Berger, I. Kocar, E. Farantatos, and A. Haddadi, "Modeling of Li-ion battery energy storage systems (BESSs) for grid fault analysis," *Electr. Power Syst. Res.*, vol. 196, Jul. 2021, Art. no. 107160.
[36] C. Zhao, P. B. Andersen, C. Træholt, and S. Hashemi, "Grid-connected battery energy storage system: A review on application and integration," *Renew. Sustain. Energy Rev.*, vol. 182, Aug. 2023, Art. no. 113400.
[37] N. Karthikeyan and A. J. G. David, "Investigation of bidirectional converter utilizing battery energy storage for an isolated load system," *Int. J. Power Electron. Drive Syst.*, vol. 14, no. 2, p. 1001, Jun. 2023.
[38] K. K. Pandey, M. Kumar, A. Kumari, and J. Kumar, "Bidirectional DC–DC buck-boost converter for battery energy storage system and PV panel," in *Proc. CoMSO*, 2021, pp. 681–693.
[39] J. John, A. Yoonus, F. Shijad, M. Aslam Mm, A. Thasneem, and L. Arun, "Isolated PV system with fuzzy logic based MPPT controller and battery management system," in *Proc. 5th Int. Conf. Electr., Electron., Commun., Comput. Technol. Optim. Techn. (ICEECCOT)*, Dec. 2021, pp. 194–199.
[40] T. A. Abdul-Jabbar, A. A. Obed, and A. J. Abid, "Battery management system with fuzzy logic controller for efficient lithium-ion usage," *AIP Conf. Proc.*, vol. 2591, no. 1, Mar. 2023, Art. no. 040013.
[41] S.-H. Ko, S. R. Lee, H. Dehbonei, and C. V. Nayar, "Application of voltage- and current-controlled voltage source inverters for distributed generation systems," *IEEE Trans. Energy Convers.*, vol. 21, no. 3, pp. 782–792, Sep. 2006.
[42] A. M. Alzahrani, M. Zohdy, and B. Yan, "An overview of optimization approaches for operation of hybrid distributed energy systems with photovoltaic and diesel turbine generator," *Electr. Power Syst. Res.*, vol. 191, Feb. 2021, Art. no. 106877.
[43] S. K. Thirumalai, A. Karthick, P. K. Dhal, and S. Pundir, "Photovoltaic-wind-battery and diesel generator-based hybrid energy system for residential buildings in smart city Coimbatore," *Environ. Sci. Pollut. Res.*, vol. 31, no. 9, pp. 14229–14238, Jan. 2024.
[44] M. Chethan and R. Kuppan, "A review of FACTS device implementation in power systems using optimization techniques," *J. Eng. Appl. Sci.*, vol. 71, no. 1, p. 18, Dec. 2024.
[45] A. Touhami, Z. S. Ahmed, and F. M. Albatsh, "Performance evaluation of fuzzy-logic controller applied to a UPFC transmission system," *Electrotehnica Electron. Autom.*, vol. 66, no. 1, pp. 122–131, 2018.
[46] M. Mauryan and V. Ramkumar, "Phasor measurement units in power system networks-a review," *Int. J. Adv. Inf. Commun. Technol.*, vol. 1, no. 1, pp. 120–125, 2014.

M. DHINU LAL received the bachelor's degree in electrical and electronics engineering from the University of Kerala, in 2009, and the master's degree in power systems engineering from Anna University, Chennai, in 2012. He is currently pursuing the Ph.D. degree in power systems with VIT University, focusing on machine learning techniques to address power system issues. His research interests include machine learning, fuzzy logic, renewable energy, micro grids power system measurements, and electro magnetics.

RAMESH VARADARAJAN (Member, IEEE) received the bachelor's degree in mechanical engineering from the Birla Institute of Technology and Science (BITS), Pilani, in 1983, the A.M.I.E. degree in electrical engineering from the Institute of Engineers, India, in 1992, the master's degree in power systems engineering from the Thiagarajar College of Engineering (TCE), Madurai Kamaraj University, in 1994, and the Ph.D. degree from VIT University, Vellore, India, in 2011. He is currently a Professor with the School of Electrical Engineering, VIT University. His current interests include machine learning, artificial intelligence, and power systems.